TÜBİTAK

Turkish Journal of Earth Sciences

http://journals.tubitak.gov.tr/earth/

Research Article

Turkish J Earth Sci
(2019) 28: 860-881

doi:10.3906/yer-1905-3

Parameter estimations from gravity and magnetic anomalies due to deep-seated faults: differential evolution versus particle swarm optimization

Yunus Levent EKİNCİ[1,2,*], Çağlayan BALKAYA[3], Gökhan GÖKTÜRKLER[4]

[1]Department of Archaeology, Faculty of Sciences and Arts, Bitlis Eren University, Bitlis, Turkey
[2]Career Application and Research Center, Bitlis Eren University, Bitlis, Turkey
[3]Department of Geophysical Engineering, Faculty of Engineering, Süleyman Demirel University, Isparta, Turkey
[4]Department of Geophysical Engineering, Faculty of Engineering, Dokuz Eylül University, İzmir, Turkey

Received: 06.05.2019 • **Accepted/Published Online:** 26.09.2019 • **Final Version:** 07.11.2019

Abstract: Estimation of causative source parameters is an essential tool in exploration geophysics and is frequently applied using potential field datasets. Naturally inspired metaheuristic optimization algorithms based on some stochastic procedures have attracted more attention during the last decade due to their capability in finding the optimal solution of the model parameters from the parameter space via direct search routines. In this study, the solutions obtained through differential evolution algorithm, a rarely used metaheuristic algorithm in geophysics, and particle swarm optimization, which is one of the most used global optimization algorithms in geophysics, have been compared in terms of robustness, consistency, computational cost, and convergence rate for the first time. Applications have been performed using both synthetic and real gravity and magnetic anomalies due to deep-seated fault structures. Before the parameter estimation studies, resolvability of the fault parameters have been examined by producing cost function/error energy topography maps to understand the suitability of the problem and also the mathematical nature of the inversion procedure. Optimum control parameters of both algorithms have also been determined via some parameter tuning studies performed on synthetic anomalies. Consequently, the tuned parameters clearly improved the effectiveness of both metaheuristics on the solution of the optimization problems under consideration. Moreover, reliabilities of the obtained solutions and also the possible uncertainties have been investigated using probability density function analyses. Real data applications have been performed using a residual gravity anomaly observed over the Graber oil field (Oklahoma, USA) and an airborne total field magnetic anomaly observed over the Perth Basin (Australia). Applications have shown that although both algorithms provided close results in both synthetic and real data experiments, the differential evolution algorithm yielded slightly better solutions in terms of robustness, consistency, computational cost, and convergence rate. Thus, the differential evolution algorithm is worth paying more attention to and is suggested as a powerful alternative to particle swarm optimization for the inversion of potential field anomalies.

Key words: Gravity and magnetic anomalies, fault structures, parameter estimation, differential evolution, particle swarm optimization, statistical analyses

1. Introduction

Due to the mathematical nature of the gravity and magnetic methods in geophysics, numerous data processing techniques are easily performed to analyze their anomalies obtained from different types of investigations changing in a wide range of varieties. Based on the objectives of the investigations, the most commonly used techniques are generally separated into two different groups. The first group techniques, involving linear transformations, directional derivative-based techniques, image enhancement procedures, spectral methods, filtering operators, etc., generally aim at exploring and locating the geological source structures causing the potential field anomalies (Büyüksaraç et al., 2005; Oruç and Keskinsezer, 2008; Xu et al., 2011; Balkaya et al., 2012; Ekinci and Yiğitbaş, 2012, 2015; Ekinci et al., 2013; Aydemir et al., 2014; Oruç et al., 2017; Boukerbout et al., 2018; Sındırgı and Özyalın, 2019; Timur et al., 2019). The second group techniques, which have a significant role in geophysics, aim at estimating the source model parameters of the causative structures through improving the fit between the observed and the calculated anomalies in successive iterations (Li and Oldenburg, 1996; Fedi and Rapolla, 1999; Salem et al., 2004; Asfahani and Tlas, 2007; Essa, 2012; Mehanee, 2014; Damaceno et al., 2017). Although the existence of many disadvantages generally originated from

* Correspondence: ylekinci@beu.edu.tr

the nonuniqueness and ill-posedness phenomena, noise content, and also the insufficient number of observed data, inversion techniques are generally successfully used in geophysical parameter estimation studies with the help of some constraints and prior information. While improving the cost/error/objective function, which is the indicator of the fitness between the observed and the calculated geophysical data, the global minimum is searched in a model space using either a global optimization or a local optimization technique (Gallardo and Meju, 2004; Tarantola, 2005; Ekinci, 2008; Ekinci and Demirci, 2008; Fernández-Martínez et al., 2010; Mehanee et al., 2011; Göktürkler and Balkaya, 2012; Biswas and Sharma, 2014; Mehanee and Essa, 2015; Alkan and Balkaya, 2018). Gradient-based local optimization techniques are known to be faster in terms of convergence rates and computational cost, but their success strongly depends on the initial guess, which should be in the close neighborhood of the global minimum (Menke, 1989; Chunduru et al., 1997; Başokur et al., 2007; Ekinci and Demirci, 2008; Maiti et al., 2011; Ogunbo, 2018). On the other hand, the success of the gradient-free global optimization algorithms does not depend on a well-constructed initial guess and they can mostly keep away from a local minimum by using some stochastic search procedures (Monteiro Santos, 2010; Pekşen et al., 2011; Sharma and Biswas, 2013; Ekinci et al., 2016, 2017; Balkaya et al., 2017; Kaftan, 2017; Essa and Elhussein, 2018). These efficient procedures make it possible to change the current position of the model parameter vector by using more global information about the misfit surface (Sen and Stoffa, 1995). In spite of the huge computational cost for inverse problems having intense forward equations, naturally inspired metaheuristic algorithms have gained more popularity during the last decade. Among the several global optimization algorithms used in model parameter estimation studies of gravity and magnetic field anomalies, the particle swarm optimization (PSO) (e.g., Srivastava and Agarwal, 2010; Toushmalani, 2013; Pallero et al., 2015, 2017; Ekinci, 2016; Singh and Biswas, 2016; Essa and Elhussein, 2018; Essa and Munschy, 2019), the genetic algorithm (GA) (e.g., Yamamoto and Seama, 2004; Montesinos et al., 2005, 2016; Chen et al., 2006; Kaftan, 2017), and the simulated annealing (SA) (e.g., Nagihara and Hall, 2001; Roy et al., 2005; Asfahani and Tlas, 2007; Tlas and Asfahani, 2011; Biswas, 2015; Biswas and Acharya, 2016; Biswas, 2017; Biswas et al., 2017) are the more popular ones. In particular, PSO is more robust and also faster in solving nonlinear problems (Duan and Liu, 2010). Furthermore, a comparative study between the PSO, GA, and SA algorithms performed using self-potential anomalies showed the efficiency and speed of PSO (Göktürkler and Balkaya, 2012). Thus, it may be stated that PSO is the preferable optimization technique used in potential field parameter estimation studies. On the other hand, recently, the differential evolution (DE) algorithm has been introduced as a powerful tool for the inversion of potential field datasets (Ekinci et al., 2016, 2017; Balkaya et al., 2017). However, the DE algorithm has not gained wide currency in geophysical studies yet. Thus, in this study, using gravity and total field magnetic datasets generated by deep-seated fault structures, an effort was made to compare the DE and PSO algorithms in terms of robustness, consistency, computational cost, and convergence characteristics. In addition to synthetically produced noise-free and noisy dataset applications, real data cases including a residual gravity anomaly from the USA and an airborne total field magnetic anomaly from Australia were used for the estimation of geological source model parameters.

2. Methodology

2.1. DE algorithm

DE is used to optimize real parameters and real-valued functions (Storn and Price, 1995, 1997; Storn, 1996). This population- and vector-based metaheuristic algorithm uses some evolutionary procedures like the GA, such as initialization, mutation, and selection stages. In DE applications, first, some essential parameters, namely population number, crossover probability, and the mutation constant (or weighting factor), are selected by the user, and then an initial population is generated (Storn, 1996). The first operation begins with the mutation, which has various approaches in DE for obtaining a donor vector (Storn and Price, 1995, 1997). Later, the evolution strategy including mutation scheme, number of difference vectors, and crossover scheme (binomial or exponential) is selected (Balkaya, 2013). The trial vector is obtained using both donor vector elements and the target vector, and the recombination process combines successful solutions considering the previous generation (Balkaya et al., 2017). In the last step, considering the lowest error/misfit values, the target vector or trial vector is transferred to the next generation (Ekinci et al., 2016, 2017). These processes in the evolution loop continue until a predefined iteration number or the reaching of a satisfactory objective function value. Here, the DE/best/1/bin strategy of the algorithm was used in every example. A brief flowchart showing the processing steps in the DE algorithm is given in Figure 1a.

2.2. PSO algorithm

PSO is the most commonly used population-based optimization algorithm for solving real-valued functions through some natural biological and sociological inspirations (Kennedy and Eberhart, 1995; Shi and Eberhart, 1998). Briefly, the algorithm is inspired by the behaviors of bird flocks and fish schools (Pallero et al., 2015). In this naturally inspired derivative-free

metaheuristic technique, the best solution involving the model parameters is sought in the model space using a particle population having random positions and velocities (Srivastava and Agarwal, 2010; Göktürkler and Balkaya, 2012; Ekinci, 2016; Singh and Biswas, 2016; Essa and Munschy, 2019). In the algorithm, the position vector of a particle describes a pilot solution (Das et al., 2008). Each particle keeps useful information about its previous best position and velocity (Essa and Elhussein, 2018). Inertia weight and the two coefficients controlling the particle's individual and social behaviors are the essential parameters for the success of the PSO technique. The updates of the velocity and position of each particle continue until reaching a predefined iteration number or obtaining a satisfactory objective function value. A brief flowchart showing the processing steps in the PSO algorithm is shown in Figure 1b.

3. Forward modeling

Over a profile across an arbitrarily magnetized fault structure (Figure 2), gravity (Radhakrishna Murty and Krishnamacharyulu, 1990) and magnetic anomalies (Radhakrishna Murty, 1998; Radhakrishna Murty et al., 2001) at any observation point are produced by using the following expressions, respectively:

$$\Delta G(x) = 2Gdc\left[\left((x-xo)\sin(\theta)-z1\cos(\theta)\right)\left(\sin(\theta)\ln(r2/r1)+\cos(\theta)(\theta2-\theta1)\right)+(z2\ \theta2-z1\ \theta1)\right] \quad (1)$$

$$\Delta T(x) = 2J'\sin(\theta)\left[\cos(\theta+\phi')(\theta2-\theta1)+\sin(\theta+\phi')\ln(r2/r1)\right] \quad (2)$$

Here, ΔG denotes the gravity anomaly, G is the gravitational constant, dc represents the density contrast, θ is the fault angle, x is the horizontal distance along the observation profile, xo denotes the origin placed above the upper corner of the fault, and z1 and z2 are the depths to the top and the bottom of the fault, respectively. ΔT is the magnetic anomaly in any component and J represents the intensity of effective magnetization. The definitions of the other terms in Eqs. (1) and (2) are given below.

$$\theta1 = \pi/2 + \arctan\left(\frac{x-xo}{z1}\right) \quad \text{for} \quad z1 \neq 0$$

$$= \pi/2\left(1+\frac{x-xo}{|x-xo|}\right) \quad \text{for} \quad z1=0, \quad x \neq 0$$

$$= \pi/2 \quad \text{for} \quad z1=0, \quad x=0 \quad (3)$$

$$\theta2 = \pi/2 + \arctan\left[\frac{(x-xo)+(z2-z1)\cot(\theta)}{z2}\right] \quad (4)$$

$$r1 = \left[(x-xo)^2+z1^2\right]^{1/2} \quad (5)$$

$$r2 = \left[\left((x-xo)+(z2-z1)\cot(\theta)\right)^2+z2^2\right]^{1/2} \quad (6)$$

$$\phi' = \phi - \arctan\left[\sin(\alpha)\cot(Dm)\right] \quad (7)$$

$$J' = J\left[1-\cos^2(\alpha)\cos^2(Dm)\right]^{1/2} \quad (8)$$

Here, ϕ denotes the dip of the effective magnetization vector, α represents the strike of the two-dimensional body measured due east or west from the magnetic north, and Dm denotes the direction of measurement and it is equal π to for the vertical component, 0 for the horizontal component, and the inclination angle of the earth's magnetic field for the total field.

4. Applications

4.1. Nature of the inverse problem

Due to the complex nature of the cost/error/objective function, which is the measure of the misfit between measured and calculated data, topographical surfaces of this function mostly exhibit multiple valleys and hills. Among these topographic changes, the valley showing the minimum error value is called the unique global minimum. The topographic nature of the global minimum also gives insight into the parameter resolvability characteristics in parameter estimation studies. Therefore, investigation of the cost function topographies is a significant task in optimization procedures. This task obviously contributes to understanding which model parameters are resolvable or not. Hence, the topographies of the cost function, namely misfit/error surfaces (error energy maps), should be produced for each pair of the model parameters before inversion studies (Ekinci et al., 2016, 2017). In order to achieve this, synthetic gravity and magnetic datasets were produced using Eqs. (1) and (2), respectively. Residual gravity (Figure 3a) and total field magnetic anomalies (Figure 3b) due to a hypothetical deep-seated fault structure were generated using the model parameters given in Tables 1 and 2, respectively. In the magnetic anomaly computation, a magnetic inclination of 60° was used. Both datasets were computed along a profile 50 km long with a sampling interval of 1 km. The following error function was considered during the optimization procedures:

$$Err = \frac{1}{N}\sum_{i=1}^{N}\left(V_i^{obs}-V_i^{cal}\right)^2 \quad (9)$$

Here, N is the number of data, and V_i^{obs} and V_i^{cal} are the observed and calculated data, respectively. Error topography contour maps were produced for each parameter pair by fixing the other parameters to the actual values. Here, selecting the true parameter as the mean value, parameter spaces having relatively narrow limits between minima and maxima were used to better observe the error surface contours around the global minima.

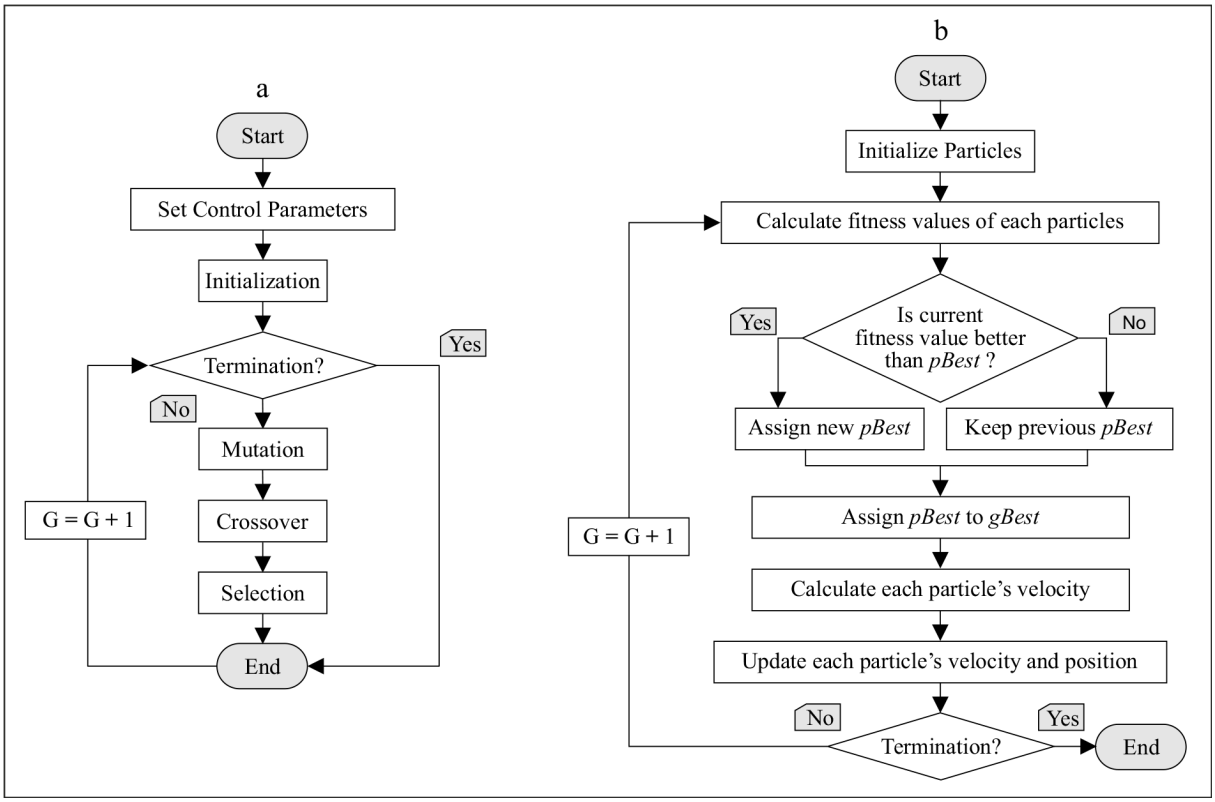

Figure 1. Flowcharts showing the main processing steps of the a) DE and b) PSO algorithms.

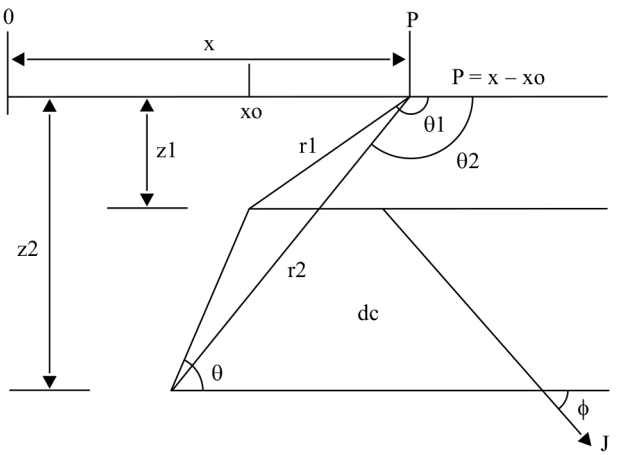

Figure 2. Deep-seated fault structure and the model parameters used in gravity and magnetic data optimizations.

Figure 4 illustrates the contour maps and the white circles overlapping them indicate the global minima in each map. These maps show the possible positions of the model parameter solutions inside the lowest error area surrounded by the minimum contour value. The shapes of the lowest error areas are the significant indicators that provide insight into the parameter resolvabilities. Figure 4 shows nearly circular contour lines surrounding the lowest error surfaces for some parameter pairs. This behavior clearly indicates that the related model parameter is uncorrelated with the other one and they can be resolved independently. The elliptical lowest surface contours sloping to one of the parameter axes indicate positive or negative correlations, which means that the parameter estimation depends on the success of the other one's estimation. In other words, in the case of the existence of a positive correlation between two model parameters, if the value of one parameter is increased, the other parameter value should be increased too for a good estimation. Contrarily, if either one is increased the other one should be decreased in the case of negative correlations between two model parameters. The sloping unclosed contour lines also indicate the dependencies of the parameter solutions. However, unclosed contour behaviors make the optimization more difficult due to the existence of equivalent solutions in the narrow valley topography having the same error values. Luckily, there are no contour lines exactly parallel to any axis in the error energy topography maps, which makes successful parameter estimations possible.

In the magnetic data case, as in the previous example, the error topography contour maps were produced for

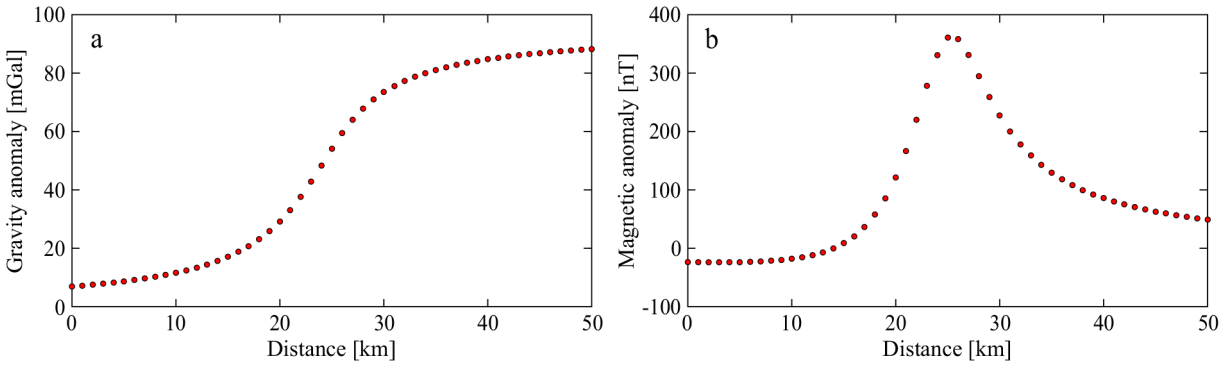

Figure 3. a) Synthetic gravity and b) synthetic magnetic anomalies due to deep-seated fault structure shown in Figure 2.

Table 1. True values and search space bounds of model parameters used in both noise-free and noisy synthetic gravity data cases.

Model parameters	True values	Search spaces	
		Min.	Max.
z1 [km]	3.00	0.10	6.00
z2 [km]	8.00	6.00	20.00
θ [°]	60.00	0.01	180.00
dc [g cm^{-3}]	0.45	0.01	1.00
xo [km]	25.00	0.01	50.00

Table 2. True values and search space bounds of model parameters used in both noise-free and noisy synthetic magnetic data cases.

Model parameters	True values	Search spaces	
		Min.	Max.
z1 [km]	3.00	0.10	6.00
z2 [km]	8.00	6.00	20.00
θ [°]	60.00	0.01	180.00
ϕ [°]	60.00	–180.00	180.00
J [nT]	200.00	1.00	1000.00
xo [km]	25.00	0.01	50.00

each parameter pair by fixing the other parameters to the actual values. Again, narrow parameter spaces were used in the computations. Figure 5 demonstrates the error energy topography maps for each parameter pair together with the related global minima marked by white circles. Since there is one more model parameter in the magnetic data case, more crowded model parameter pairs are seen in this instance. Unlike the gravity data case (Figure 4), only one map exhibiting unclosed contours around the global minimum exists. Most of the error topography maps show nearly circular closed contours that specify the lowest error areas, showing the resolvability of the parameter pairs independently. Positive or negative correlations between some parameter pairs are also identified by the existence of elliptical contour lines sloping to one of the parameter axes. Only one parameter pair shows unclosed contours around the global minimum, which indicates its challenging mathematical nature against the DE and PSO algorithms. Contour lines parallel to any axis are not observed in the error topography maps. The analyses presented in this section clearly show that the effortful mathematical natures of the inverse problems of the gravity and magnetic anomalies due to fault structures in our case are reasonable choices for the comparison tests for the efficiencies of the DE and PSO algorithms.

4.2. Tuning and parameter estimations through synthetic data

It is well known that every nature-inspired global optimization algorithm has its own control parameters, which largely affect the convergence behavior of the inversion procedure. These parameters are vital for the success of the optimization and their selection depends on the nature of the problem under consideration. Therefore, parameter tuning studies should be performed before the parameter estimations performed by global optimization algorithms (Fernandez-Martinez et al., 2010; Pekşen et al., 2014; Ekinci et al., 2016, 2017; Balkaya et al., 2017; Alkan and Balkaya, 2018) even though they are time-consuming (Eiben and Smith, 2011).

In the synthetic gravity and magnetic data experiments, quite wide search space bounds for fault model parameters (Tables 1 and 2) were used in order to test the limits of the DE and PSO algorithms. Here, first the gravity data (Figure 3a) problem was examined using some statistical results. The minimum, maximum, mean, and standard

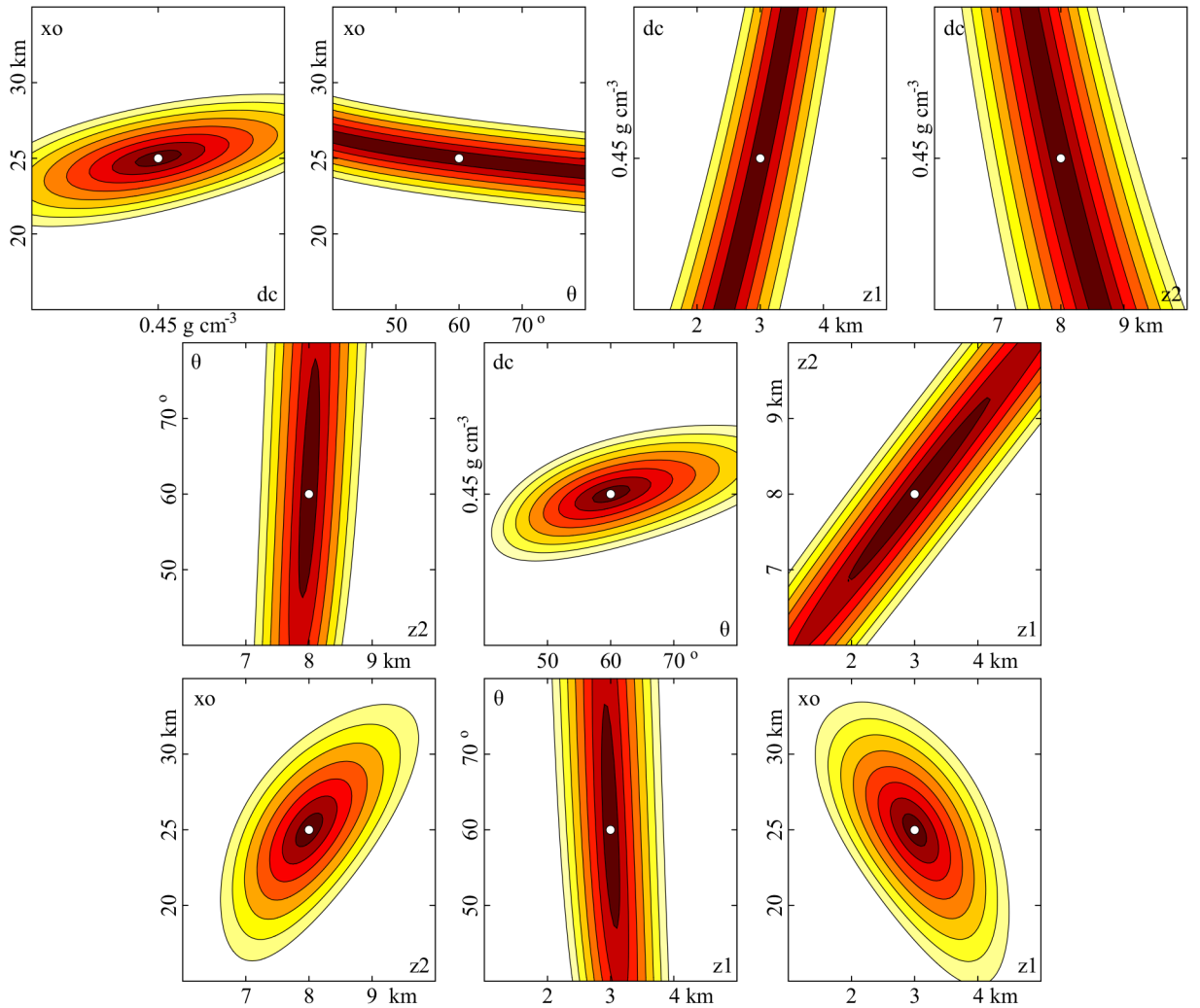

Figure 4. Error energy topography contour maps for each gravity model parameter pair. The model parameters are depicted at the end of the axes. White circles indicate the global minima of each topographic subplot.

deviation (SD) of error values obtained from a number of independent runs were taken into consideration for statistical analyses. DE tuning studies for the determination of optimum control parameters were carried out with some pairs of mutation constants and crossover probabilities. Twenty independent runs were carried out by fixing the population number to 150 (number of model parameters × 30) with 300 generations (iterations) for the optimization. The best solutions of 36 parameter pairs were obtained by applying this procedure (Table 3). Only three control parameter pairs, highlighted by boldface, produced the optimum solution having the same error values with a standard deviation of 0. This means that the same solutions including the model parameters were obtained in every run using these control parameter pairs. Thus, a more robust and efficient optimization can be performed by using these control parameters in the presented gravity data case. Additionally, a finding that attracts attention is the large error value difference between the control parameter pairs that produced the best and the worst solutions. This difference (about 8500 times) strongly affects the solution regarding the accuracy of the optimized model parameters. Hence, the importance of parameter tuning studies when using global optimization algorithms is clearly observed in this example. Based on the results listed in Table 3, 0.5 and 0.8 were considered to be the optimum values for mutation constant and crossover probability, respectively, in DE optimization for the gravity data case presented here.

PSO tuning studies were performed with the same synthetic residual gravity anomaly (Figure 3a) using some previously suggested control parameter sets including the inertia weight and the two coefficients controlling the particle's individual and social behaviors. As in the DE application, 20 independent runs were carried out for

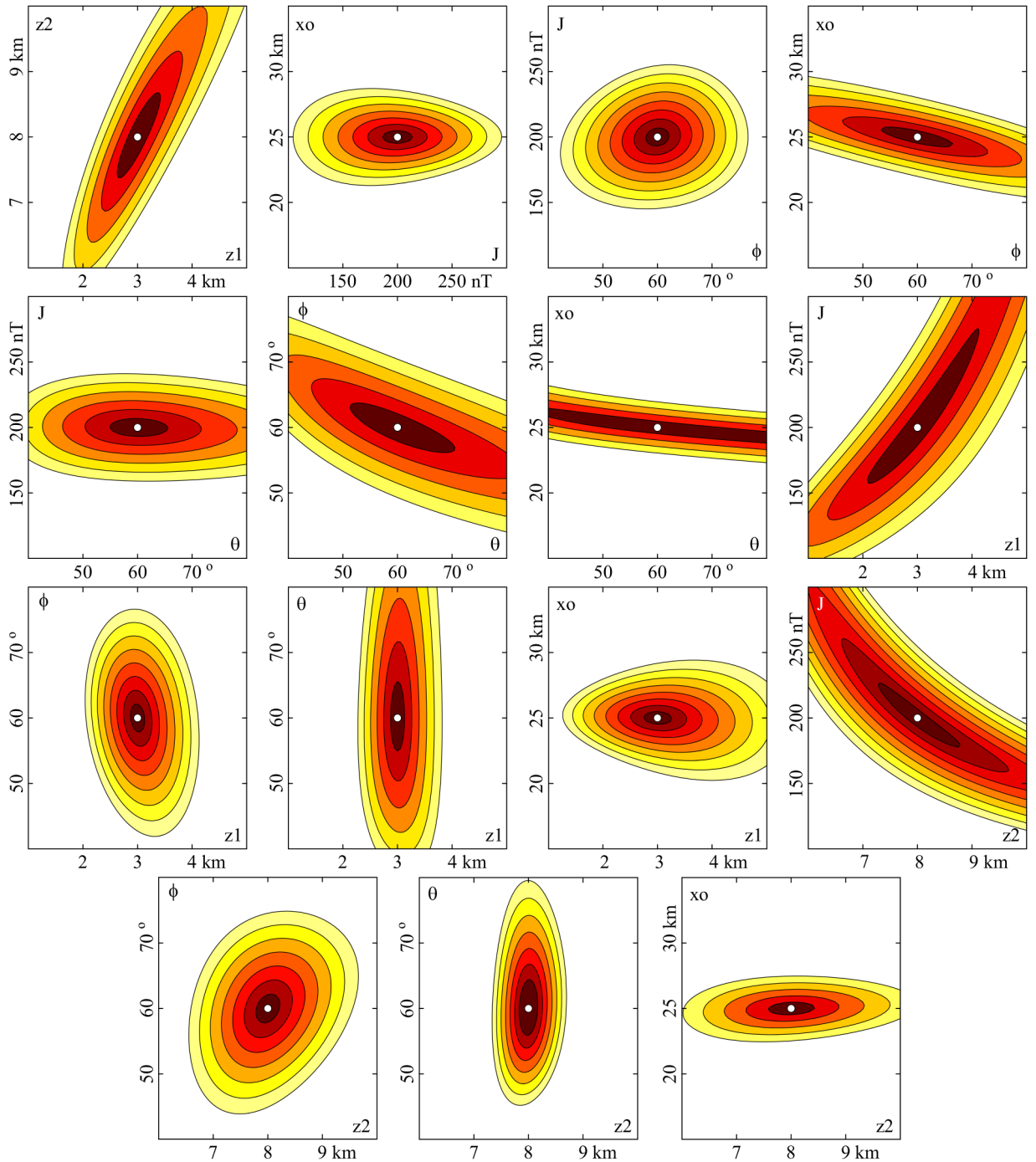

Figure 5. Error energy topography contour maps for each magnetic model parameter pair. The model parameters are depicted at the end of the axes. White circles indicate the global minima of each topographic subplot.

each control parameter set using the search space bounds listed in Table 1. Optimization procedures were performed by fixing NP to 150 (number of model parameters × 30) with 300 generations. The boldfaced optimum statistical solution having the minimum error value and SD (Table 4) was obtained with the control parameters suggested by Carlisle and Dozier (2001). It must be noted that the error value of the worst solutions is about 136 times higher than the error value of the best solution.

The best solutions obtained via the optimum control parameters of DE and PSO are given in Table 5. Both algorithms produced very close best solutions in terms of

Table 3. Parameter tuning of the DE algorithm for the synthetic noise-free gravity data case. Cr and F represent the crossover probability and the mutation constant, respectively.

F	Cr	Error [mGal]				F	Cr	Error [mGal]			
		Min.	Max.	Mean	SD			Min.	Max.	Mean	SD
0.4	0.4	0.00769	0.17770	0.09808	0.06781	0.7	0.4	0.07047	0.13847	0.11394	0.02760
	0.5	0.00008	0.15054	0.03864	0.06406		0.5	0.03634	0.17302	0.09278	0.05631
	0.6	0.00002	0.13756	0.03324	0.05914		0.6	0.00156	0.13427	0.06936	0.05072
	0.7	0.00002	0.05292	0.02103	0.02876		0.7	0.00011	0.00047	0.00035	0.00014
	0.8	0.00002	0.02665	0.00711	0.01156		0.8	0.00002	0.00003	0.00002	~0
	0.9	0.00208	0.15112	0.04441	0.06428		0.9	0.00002	0.00002	0.00002	~0
0.5	0.4	0.02558	0.12006	0.07901	0.04494	0.8	0.4	0.16517	0.29551	0.21617	0.05451
	0.5	0.00866	0.16743	0.05667	0.06611		0.5	0.04423	0.13855	0.08997	0.04082
	0.6	0.00002	0.10684	0.02617	0.04624		0.6	0.01537	0.13103	0.06493	0.04813
	0.7	**0.00002**	**0.00002**	**0.00002**	**0**		0.7	0.00129	0.06011	0.02375	0.02403
	0.8	**0.00002**	**0.00002**	**0.00002**	**0**		0.8	0.00004	0.00318	0.00109	0.00135
	0.9	0.00002	0.00935	0.00424	0.00413		0.9	0.00002	0.00003	0.00003	~0
0.6	0.4	0.05849	0.14994	0.09282	0.03477	0.9	0.4	0.16974	0.22229	0.20092	0.02447
	0.5	0.00765	0.08997	0.04669	0.03636		0.5	0.11316	0.21772	0.18696	0.04258
	0.6	0.00019	0.00903	0.00253	0.00367		0.6	0.09123	0.18255	0.14681	0.03823
	0.7	0.00002	0.00002	0.00002	~0		0.7	0.01058	0.16281	0.06253	0.06413
	0.8	**0.00002**	**0.00002**	**0.00002**	**0**		0.8	0.00108	0.02331	0.00602	0.00969
	0.9	0.00008	0.00112	0.00041	0.00018		0.9	0.00003	0.00031	0.00014	0.00011

Table 4. Parameter tuning of the PSO algorithm for the synthetic noise-free gravity data case. Set 1: Kennedy and Eberhart (1995), Set 2: Shi and Eberhart (1998), Set 3: Eberhart and Shi (2000), Set 4: Carlisle and Dozier (2001), Set 5: Trelea (2003), Set 6: Jiang et al. (2007), Set 7: Fernandez-Martinez et al. (2010), Set 8: Pekşen et al. (2014).

Optimization	Error [mGal]			
parameters	Min.	Max.	Mean	SD
Set 1	1.88812	4.77770	2.95303	1.16724
Set 2	0.20974	0.53621	0.34133	0.14453
Set 3	0.06193	0.21338	0.15183	0.06809
Set 4	**0.01383**	**0.29729**	**0.11408**	**0.08278**
Set 5	0.06809	0.18361	0.13458	0.03112
Set 6	0.06090	0.21705	0.10959	0.06398
Set 7	0.06398	0.68388	0.44977	0.18143
Set 8	0.13031	0.57008	0.27755	0.18127

model parameter accuracy, and since there is no perceptible difference between the calculated anomalies using the best model parameters obtained from the DE and PSO, only one calculated dataset is shown in Figure 6a. However, the effectiveness of the DE algorithm is seen from the mean parameter values obtained from 20 independent runs (Table 5). Unlike PSO, although starting with different positions in the model space, DE reached the same solution in every independent run, which may be particular to this example. Additionally, the error function values versus generation numbers obtained from both algorithms show that the DE algorithm provided the best solution sooner than the PSO algorithm (Figure 6b). The rapid drop of the error values in the first generations shows the faster convergence rate of the DE algorithm. Moreover, less computational cost behavior is the superiority of the DE algorithm over the PSO algorithm (Table 5). When considering all error function values obtained from 20 independent runs, the consistency of the DE algorithm is clearly seen (Figure 6c). Since the DE algorithm yielded the same model parameter

Table 5. Estimated model parameters through the DE and PSO algorithms for the synthetic gravity data cases. Best and mean represent the optimum and mean solutions obtained from 20 independent runs.

Model parameters	Estimated values							
	Noise-free case				Noisy case			
	DE		PSO		DE		PSO	
	Best	Mean	Best	Mean	Best	Mean	Best	Mean
z1 [km]	3.00	3.00	3.04	2.93 ± 0.58	3.20	3.23 ± 0.08	3.06	3.02 ± 0.75
z2 [km]	8.00	8.00	7.99	8.25 ± 0.79	8.52	8.47 ± 0.11	8.68	8.78 ± 1.02
θ [°]	60.00	60.00	61.15	68.67 ± 9.46	112.23	112.41 ± 0.64	111.32	119.10 ± 42.28
dc [g cm^{-3}]	0.45	0.45	0.46	0.45 ± 0.13	0.43	0.43 ± 0.02	0.41	0.44 ± 0.16
xo [km]	25.00	25.00	24.93	24.58 ± 0.30	22.80	22.81 ± 0.02	22.80	22.90 ± 0.18
Error [mGal]	0.00002		0.01383		1.94		1.94	
CPU time (s)	98.50		478.30		94.50		487.10	

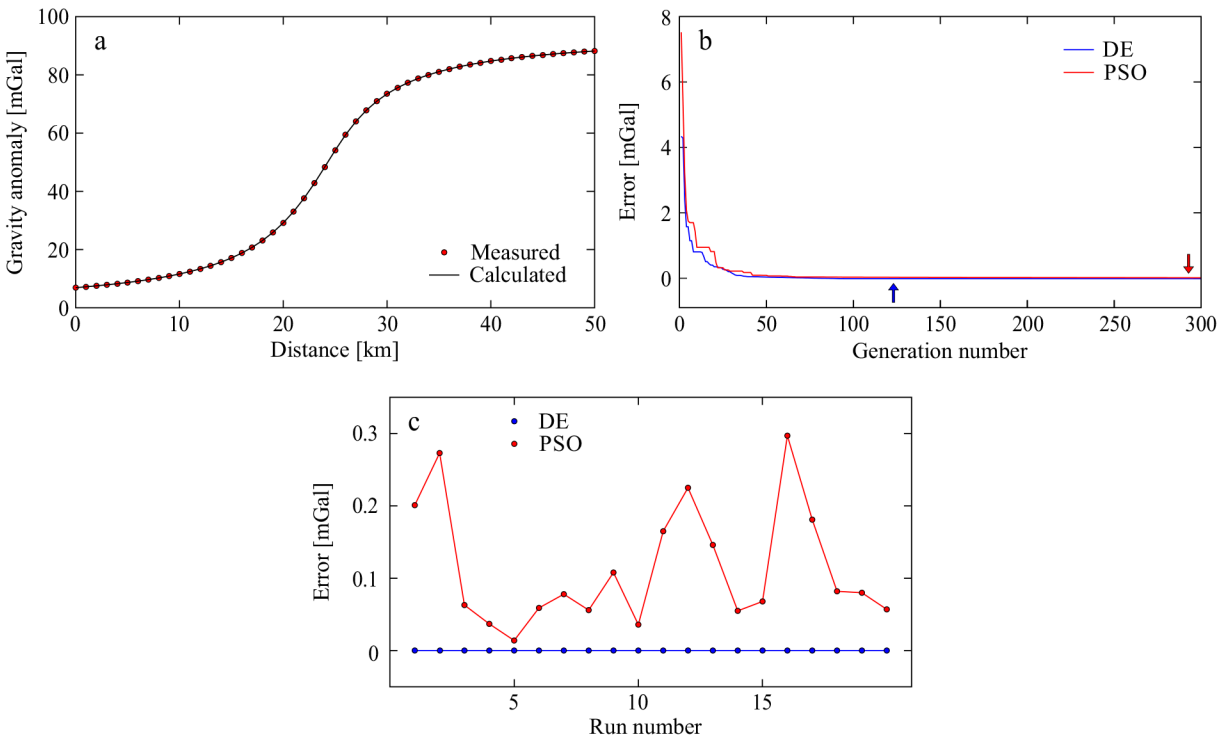

Figure 6. a) The fit between the synthetic noise-free gravity data and the calculated gravity data obtained from best-fitting model parameters. It must be noted that the DE and PSO algorithms produced almost identical calculated anomalies. b) The change of the error values versus generation number. The arrows show the generation numbers at which the best solutions were obtained. c) The error values obtained from 20 independent runs through DE and PSO algorithms.

values in every independent run, statistical analyses were performed only for the estimated parameters by the PSO algorithm. These statistical analyses included determining the characteristics of probability distributions of model input achieved by using the best solutions obtained from 20 independent runs of the algorithm. The probability density function (PDF) between 95% confidence interval limits, confidence interval limits of mean parameter values with a probability of 95% together with mean values calculated for each model parameter, and the best

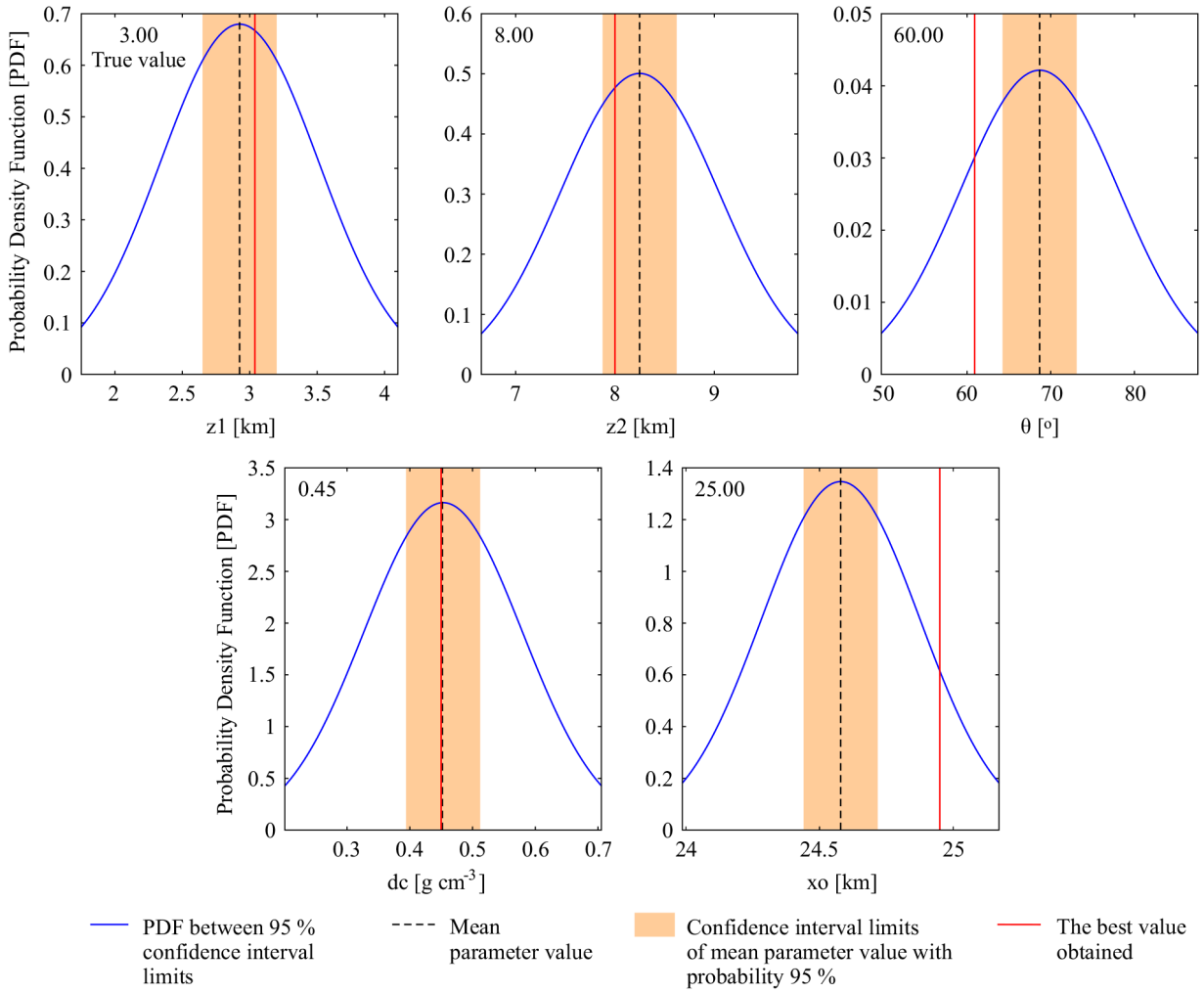

Figure 7. Probability density function analyses of the best model parameter values obtained in 20 independent runs via PSO algorithm for the noise-free gravity data example. True values of the model parameters are also indicated on each plot.

parameter values predicted by the algorithm are shown in Figure 7. Relatively narrow intervals from the best solutions of each parameter were obtained for the PSO results. However, it must be noted that two parameters (θ and xo) are not within the confidence interval limits (Figure 7). Thus, it is observed that the DE algorithm showed a more robust and steadier characteristic in the noise-free gravity data case. In the next step, a Gaussian noise involving pseudorandom numbers, which represent about 5% of the data, was added to the synthetic data (Figure 8a). Estimated model parameters through both algorithms for the noisy synthetic gravity data case are listed in Table 5. Although there are slight differences between the best model parameters obtained by the PSO and DE algorithms, they produced almost the same anomaly response (Figure 8a) having the same error values (Table 5). However, the mean parameter values obtained through the DE algorithm have remarkably lower SDs. The faster convergence rate of the DE algorithm is seen once again (Figure 8b). The error values obtained from every run for both algorithms are illustrated in Figure 8c. More consistent solutions were obtained through the DE algorithm. Additionally, based on the PDF plots, all model parameter values obtained via the DE algorithm are within the confidence interval (Figure 9), while one parameter value (xo) obtained by the PSO algorithm has some uncertainties (Figure 10). According to these findings, the DE algorithm is the victor of this round.

Inversion of total field magnetic anomaly (Figure 3b) was also performed by applying the same procedures given before. Only the number of the population was increased to 180, due to the existence of 6 model parameters (number of model parameters × 30). The best solutions of each parameter pair are listed in Table 6. Two parameter pairs, highlighted by boldface, produced the best solutions having the same statistical

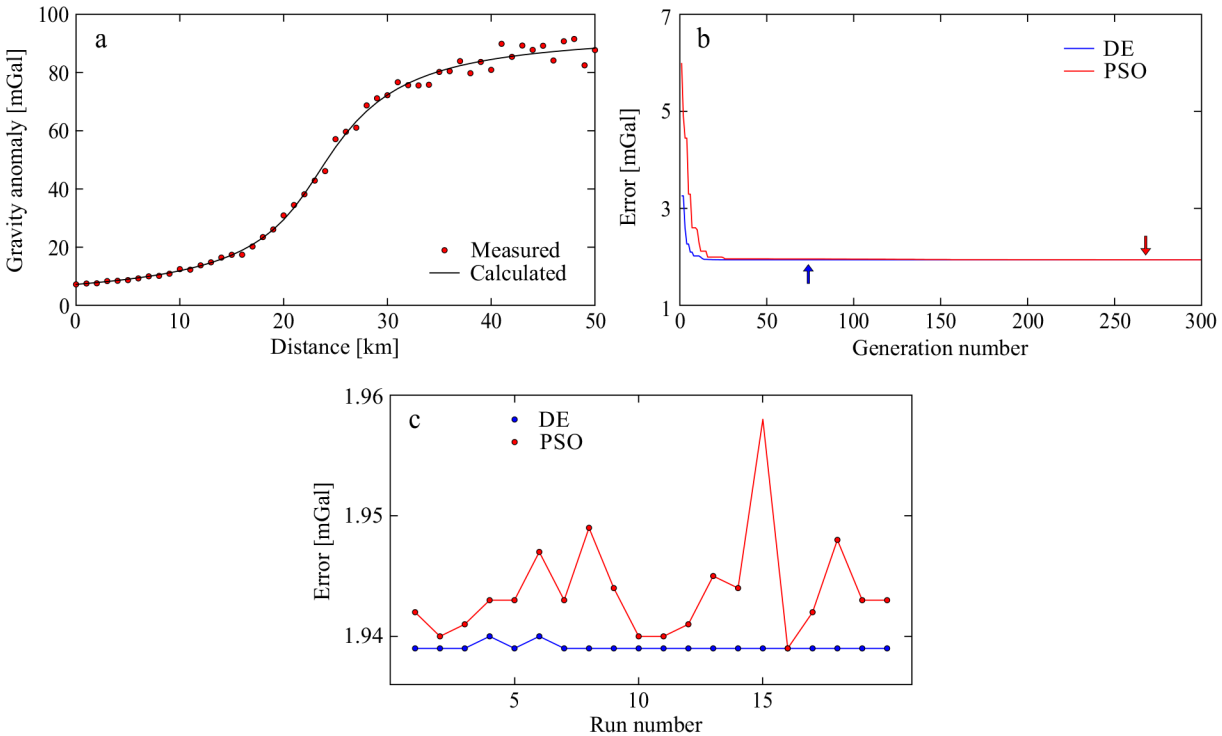

Figure 8. a) The fit between the synthetic noisy gravity data and the calculated gravity data obtained from best-fitting model parameters. It must be noted that the DE and PSO algorithms produced almost identical calculated anomalies. b) The change of the error values versus generation number. The arrows show the generation numbers at which the best solutions were obtained. c) The error values obtained from 20 independent runs through DE and PSO algorithms.

results. The large difference between the error values of the best and the worst solutions showed the importance of tuning studies once again. For the magnetic data case, the values of 0.5 and 0.8 were determined for the optimum mutation constant and crossover probability, respectively. Table 7 shows the results of PSO performed through various control parameters. As in the gravity data example, the control parameters suggested by Carlisle and Dozier (2001) produced the optimum solution, which is highlighted by boldface. Calculated magnetic model parameters via the best control parameters of the DE and PSO algorithms are given in Table 8. These algorithms produced nearly identical solutions. The fit between the optimization output and the synthetic magnetic data is exhibited in Figure 11a. The faster convergence skill of DE, characterized by a sudden drop in the error values in the early generations (Figure 11b), showed the advantage of the algorithm. As in the noise-free gravity data example, the DE algorithm yielded the same best model parameter values in every independent run, showing its robustness (Figure 11c). Since PSO produced slightly different solutions in 20 independent runs (Figure 11c), PDF plots were produced for each model parameter (Figure 12). It is seen that some model parameter values are not within the confidence interval limits, which indicates possible uncertainties in the estimations. The same amount of Gaussian noise was added to the synthetic magnetic data (Figure 13a). Estimated model parameters for both algorithms for the noisy synthetic magnetic data case are listed in Table 8. The same error values were obtained at the end of the optimization processes, but DE yielded a faster convergence rate again (Figure 13b). Moreover, the DE algorithm produced the same solution having the same error value in every independent run (Table 8; Figure 13c). Although PDF subplots show that the model parameters obtained via the PSO algorithm are within the confidence interval limits (Figure 14), the DE algorithm showed more robust and consistent characteristics in parameter estimations studies, like in the previous examples. It must be also noted that PSO produced satisfactory solutions in both noise-free and noisy magnetic data examples by using the best values, but the significant SD values of the mean parameter values obtained from 20 independent runs (Table 8) seemed to be the weaker side of the PSO algorithm in our cases. Thus, the DE algorithm is again victorious by far.

4.3. Optimizations through real data

After deciding that the DE algorithm was more successful and robust in the presented synthetic data cases, the skills

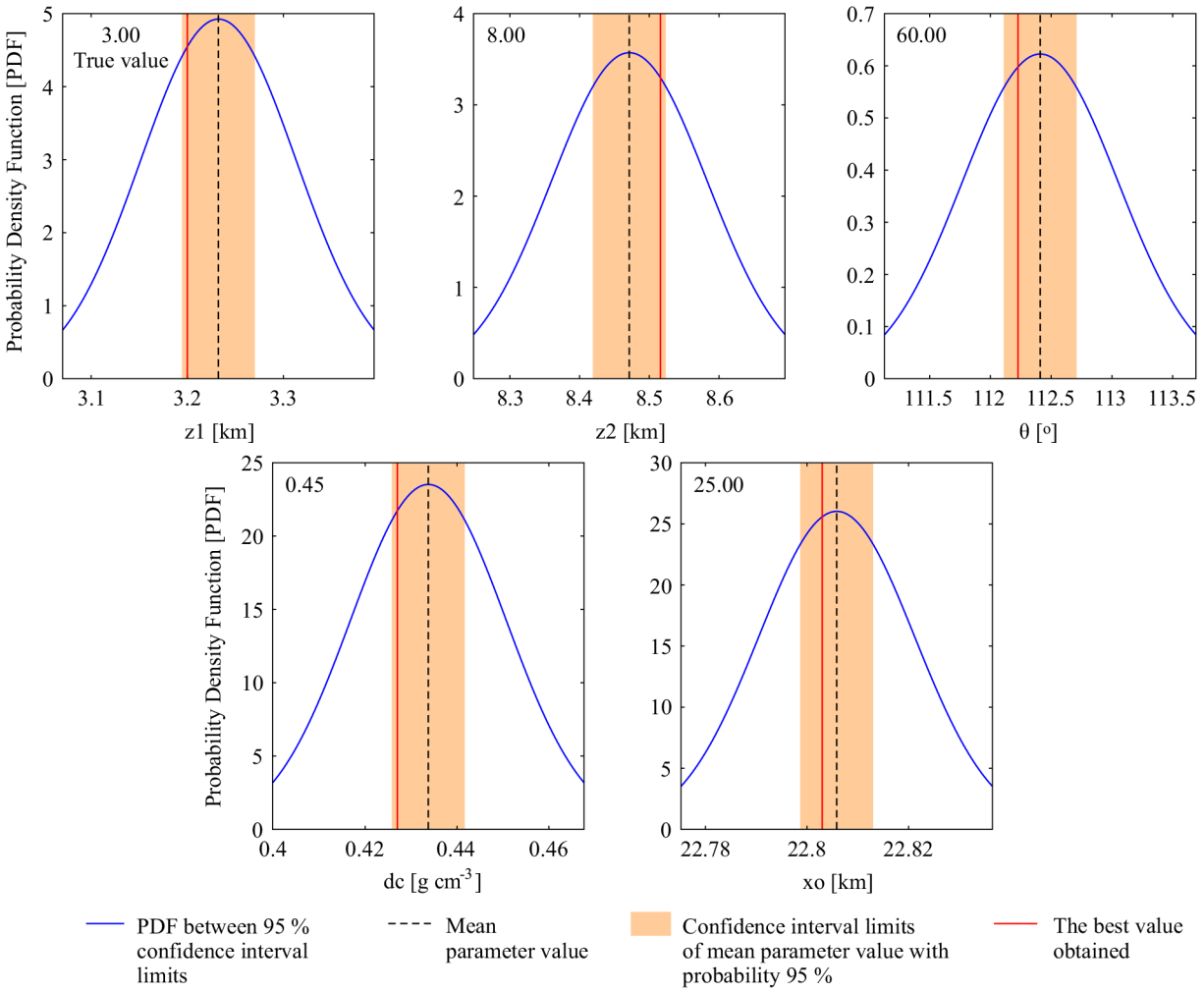

Figure 9. Probability density function analyses of the best model parameter values obtained in 20 independent runs via DE algorithm for the noisy gravity data example. True values of the model parameters are also indicated on each plot.

of both algorithms were tested again using known real gravity and magnetic anomalies. Real data optimization studies were carried out using a residual gravity anomaly observed over the Graber oil field (Oklahoma, USA) and an airborne total field magnetic anomaly observed over the Perth Basin (Australia).

4.3.1. Garber oil field gravity anomaly

Garber (USA), located on a major geologic structure, is one of the significant oil fields in the state of Oklahoma (Ferris, 1987). In addition to many anticlinal folds and many minor faults in the surroundings, the oil field is faulted by the major Nemaha fault (Ferris, 1987). Grant and West (1965) reported a deep-seated fault structure for the origin of this gravity anomaly. Gravity data along a profile 20 km long (Radhakrishna Murty and Krishnamacharyulu, 1990) were digitized using a 0.5-km sampling interval. Optimization procedures were performed using the best control parameters determined previously in the synthetic gravity data case. As in the synthetic data cases, 20 independent runs were performed using a population number of 150 and 300 generations. Search space ranges for the model parameters together with the estimated values are given in Table 9. As is clearly seen, DE and PSO applications yielded reasonable best solutions that are very close to each other, and they produced almost the same calculated anomaly naturally. A quite good fit between the observed and the calculated anomalies was achieved (Figure 15a). This gravity anomaly was studied by some researchers before. Radhakrishna Murty and Krishnamacharyulu (1990) analyzed the gravity anomaly using a damped least-squares inversion procedure and they estimated model parameters of the fault structure. Malleswara Rao et al. (2003) estimated those model parameters using a generalized inversion technique via a singular value decomposition technique. Table 9 indicates that the nature-inspired global optimization algorithms

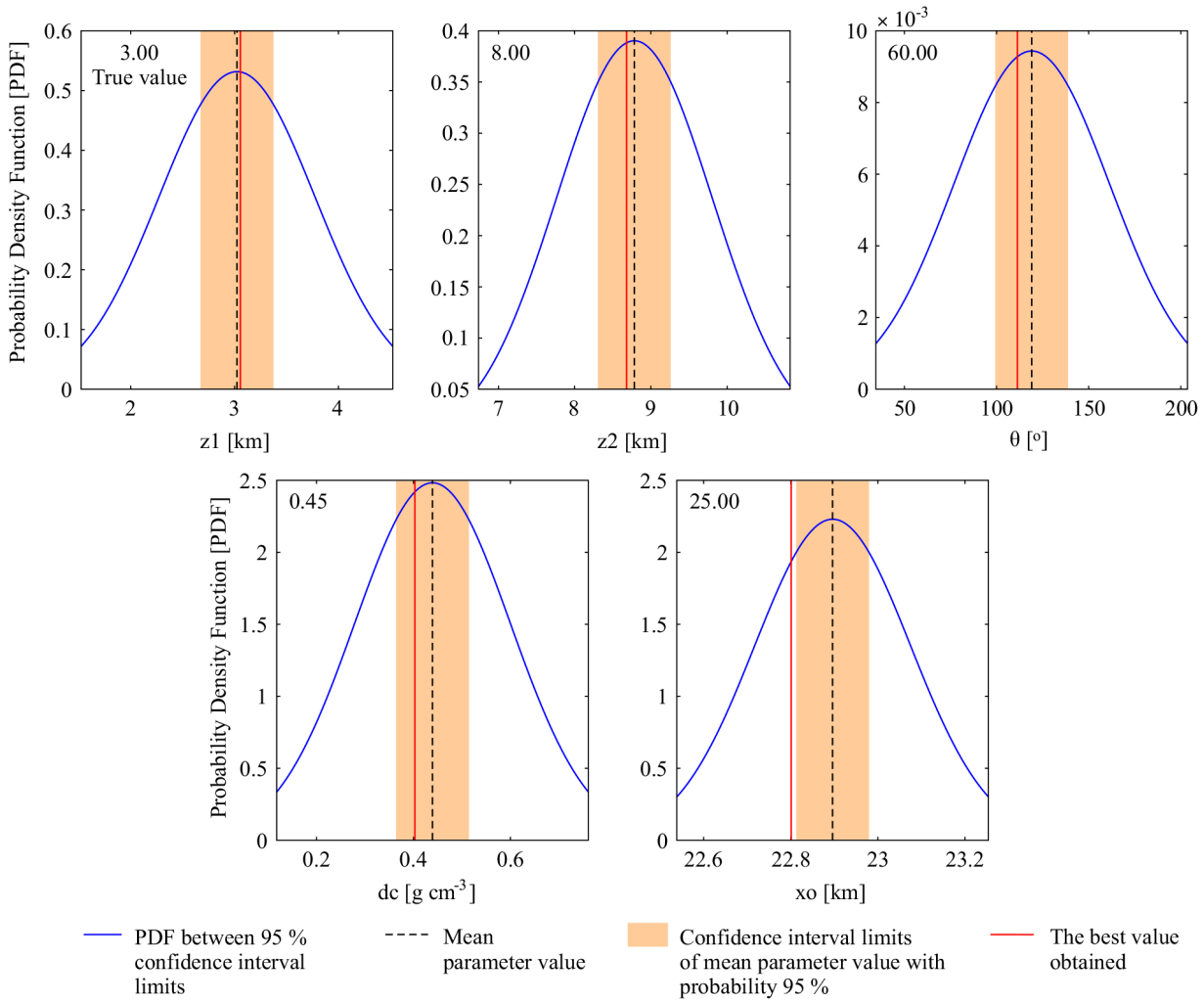

Figure 10. Probability density function analyses of the best model parameter values obtained in 20 independent runs via PSO algorithm for the noisy gravity data example. True values of the model parameters are also indicated on each plot.

used here produced results similar to previously published ones, in particular the ones obtained by Malleswara Rao et al. (2003). Considering the error values versus generation number plot (Figure 15b), DE reached the optimum solution before the 50th generation, whereas the optimum solution was obtained after the 150th generation by PSO. This real data case revealed that although both global optimization algorithms provide very close best results, the DE algorithm yields slightly better solutions in terms of computational cost and convergence characteristics. The minimum error values obtained from every independent run of the DE and PSO applications (Figure 15c) indicate that the DE algorithm displayed more consistent and robust characteristics. Additionally, the mean values of the model parameters obtained from 20 independent runs show that the SD values of the outputs of the DE algorithm are remarkable lower than those of the PSO algorithm (Table 9). Therefore, it is worth mentioning that more reliable and efficient solutions were obtained with the DE algorithm in this real gravity data case.

4.3.2. Perth Basin magnetic anomaly

In the second real data example, a total field magnetic anomaly observed over the Perth Basin (Australia) was used. The north to north-northwest trending basin is a major rift structure lying throughout the southwestern margin of Australia (Qureshi and Nalaye, 1978). Based on the prior information obtained from the structural geology of the region and drill-hole data, the magnetic anomaly was reported to be caused by a deep-seated north-south striking fault (Qureshi and Nalaye, 1978). A 40-km-long total field magnetic anomaly (Radhakrishna Murthy et al., 2001) over the fault structure was digitized with data spacing of 1 km. The DE and PSO algorithms were performed using their best control parameters determined before in the synthetic magnetic data case. The wide search space bounds used by

Table 6. Parameter tuning of the DE algorithm for the synthetic noise-free magnetic data case. Cr and F represent the crossover probability and the mutation constant, respectively.

F	Cr	Error [nT]				F	Cr	Error [nT]			
		Min.	Max.	Mean	SD			Min.	Max.	Mean	SD
0.4	0.4	0.05130	1.74502	0.76203	0.61012	0.7	0.4	0.98231	2.51349	1.71098	0.69321
	0.5	0.00042	0.02024	0.00612	0.00811		0.5	0.28201	2.19607	0.95541	0.84289
	0.6	0.00003	0.00021	0.00006	0.00007		0.6	0.04005	0.15019	0.11702	0.03991
	0.7	0.00003	0.00003	0.00003	~0		0.7	0.00051	0.02991	0.01219	0.01221
	0.8	0.00003	0.00003	0.00003	~0		0.8	0.00002	0.00003	0.00003	~0
	0.9	0.04241	1.51039	0.54387	0.63135		0.9	0.00003	0.00003	0.00003	~0
0.5	0.4	0.04398	2.29191	0.83247	0.92178	0.8	0.4	1.01032	2.04279	1.52381	0.37354
	0.5	0.00532	0.79697	0.19318	0.34295		0.5	0.43102	2.22014	1.26705	0.79147
	0.6	0.00003	0.00162	0.00062	0.00081		0.6	0.18439	1.05031	0.37081	0.38023
	0.7	**0.00003**	**0.00003**	**0.00003**	**0**		0.7	0.01782	0.10016	0.04047	0.03661
	0.8	**0.00003**	**0.00003**	**0.00003**	**0**		0.8	0.00044	0.01819	0.00511	0.00778
	0.9	0.00003	0.28032	0.06007	0.12047		0.9	0.00003	0.00004	0.00003	~0
0.6	0.4	0.24015	0.92105	0.46104	0.31265	0.9	0.4	1.37741	2.73812	2.11021	0.49219
	0.5	0.02961	0.84191	0.27412	0.35279		0.5	1.09286	2.48631	1.85941	0.59921
	0.6	0.00201	0.48039	0.11377	0.21431		0.6	0.39498	1.77912	0.91251	0.56265
	0.7	0.00003	0.00005	0.00003	~0		0.7	0.24721	0.66423	0.48291	0.15108
	0.8	0.00003	0.00004	0.00003	~0		0.8	0.02136	0.14317	0.05921	0.04972
	0.9	0.00003	0.00003	0.00003	~0		0.9	0.00054	0.00473	0.00152	0.00161

Table 7. Parameter tuning of the PSO algorithm for the synthetic noise-free magnetic data case. Set 1: Kennedy and Eberhart (1995), Set 2: Shi and Eberhart (1998), Set 3: Eberhart and Shi (2000), Set 4: Carlisle and Dozier (2001), Set 5: Trelea (2003), Set 6: Jiang et al. (2007), Set 7: Fernandez-Martinez et al. (2010), Set 8: Pekşen et al. (2014).

Optimization	Error [nT]			
parameters	Min.	Max.	Mean	SD
Set 1	3.20152	21.07902	8.89302	7.24341
Set 2	1.26381	20.23183	8.57636	8.53764
Set 3	0.04825	2.06319	0.74286	0.80277
Set 4	**0.01418**	**2.42661**	**0.73562**	**0.78365**
Set 5	0.12875	2.76161	1.66647	1.36801
Set 6	0.26459	3.19548	1.26175	1.18208
Set 7	2.28656	10.16027	6.56111	3.01192
Set 8	2.35011	7.13995	4.21788	1.77614

both algorithms are given in Table 10. After performing 20 independent runs with population and generation numbers of 180 and 300, respectively, the DE and PSO algorithms produced close results (Table 10) and also the same anomaly response. A very satisfactory correlation is clearly seen between the observed and the one produced from the best fitting model parameters (Figure 16a). This magnetic anomaly was investigated via different processing techniques before. Qureshi and Nalaye (1978) estimated the top and bottom depths of this fault structure through some analytical approaches and master curves. Radhakrishna Murthy et al. (2001) reported the depths to the top and bottom of the fault structure by using a damped least-squares inversion procedure. Both DE and PSO algorithms yielded geologically reasonable results, which are relatively in agreement with the findings of the previous studies mentioned above (Table 10). Faster convergence rate to the optimum solution (Figure 16b) and less computational cost behavior (Table 10) of the DE algorithm were observed

Table 8. Estimated model parameters through the DE and PSO algorithms for the synthetic magnetic data cases. Best and mean represent the optimum and mean solutions obtained from 20 independent runs.

Model parameters	Estimated values							
	Noise-free case				Noisy case			
	DE		PSO		DE		PSO	
	Best	Mean	Best	Mean	Best	Mean	Best	Mean
z1 [km]	3.00	3.00	3.00	3.21 ± 0.42	2.65	2.65	2.66	2.87 ± 0.85
z2 [km]	8.00	8.00	8.01	7.69 ± 0.66	8.24	8.24	8.21	8.02 ± 1.82
θ [°]	60.00	60.00	60.06	58.90 ± 2.81	54.10	54.10	53.86	83.48 ± 30.69
ϕ [°]	60.00	60.00	60.01	59.42 ± 1.22	61.26	61.26	61.25	48.15 ± 32.83
J [nT]	200.00	200.00	199.51	240.19 ± 80.07	174.53	174.53	175.74	194.54 ± 25.55
xo [km]	25.00	25.00	25.00	24.95 ± 0.09	25.17	25.17	25.18	25.07 ± 0.26
Error [nT]	0.00003		0.01		5.67		5.67	
CPU time (s)	124.50		636.30		124.80		625.10	

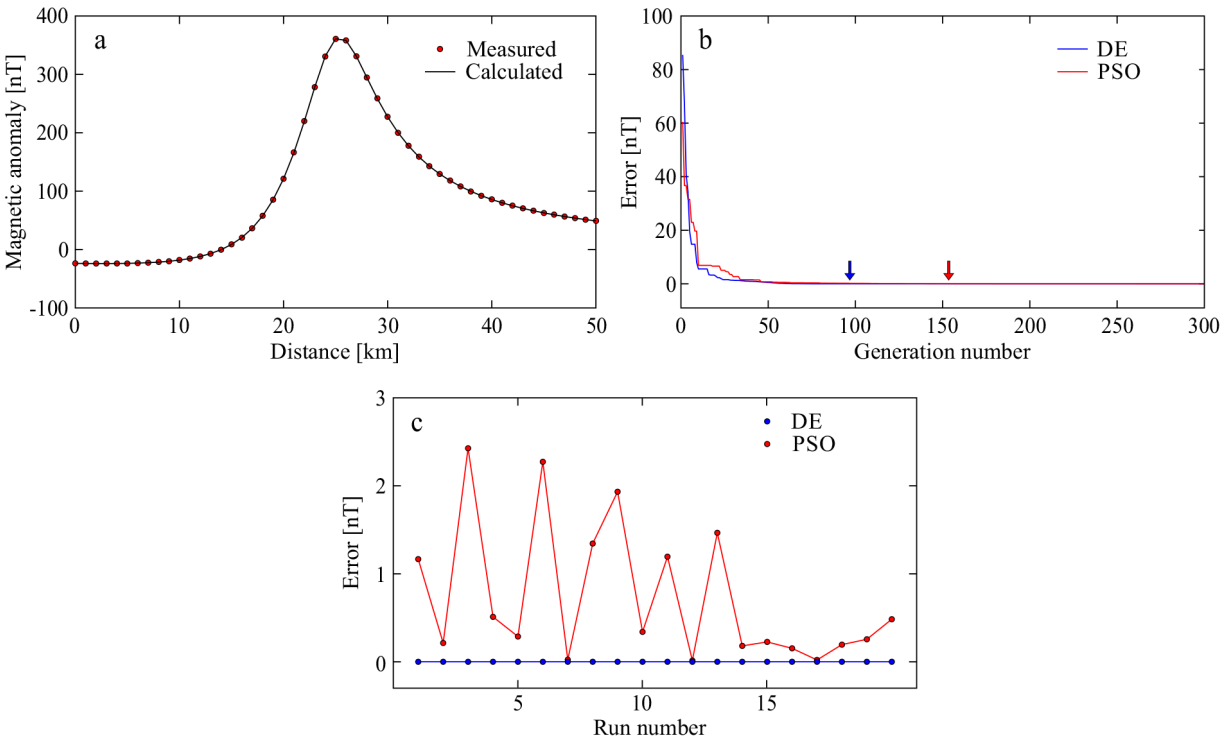

Figure 11. a) The fit between the synthetic noise-free magnetic data and the calculated magnetic data obtained from best-fitting model parameters. It must be noted that the DE and PSO algorithms produced almost identical calculated anomalies. b) The change of the error values versus generation number. The arrows show the generation numbers at which the best solutions were obtained. c) The error values obtained from 20 independent runs through DE and PSO algorithms.

once again. Additionally, the DE algorithm produced the same model parameter values (Table 10) and therefore the same error values (Figure 16c) in every independent run, showing its more robust and consistent characteristics. On the other hand, Table 10 shows the existence of considerable SD values in the mean values of the model parameters obtained from 20 independent runs of the PSO algorithm (Table 8). Therefore, the DE algorithm produced more efficient solutions in this real magnetic data case, like the previous examples.

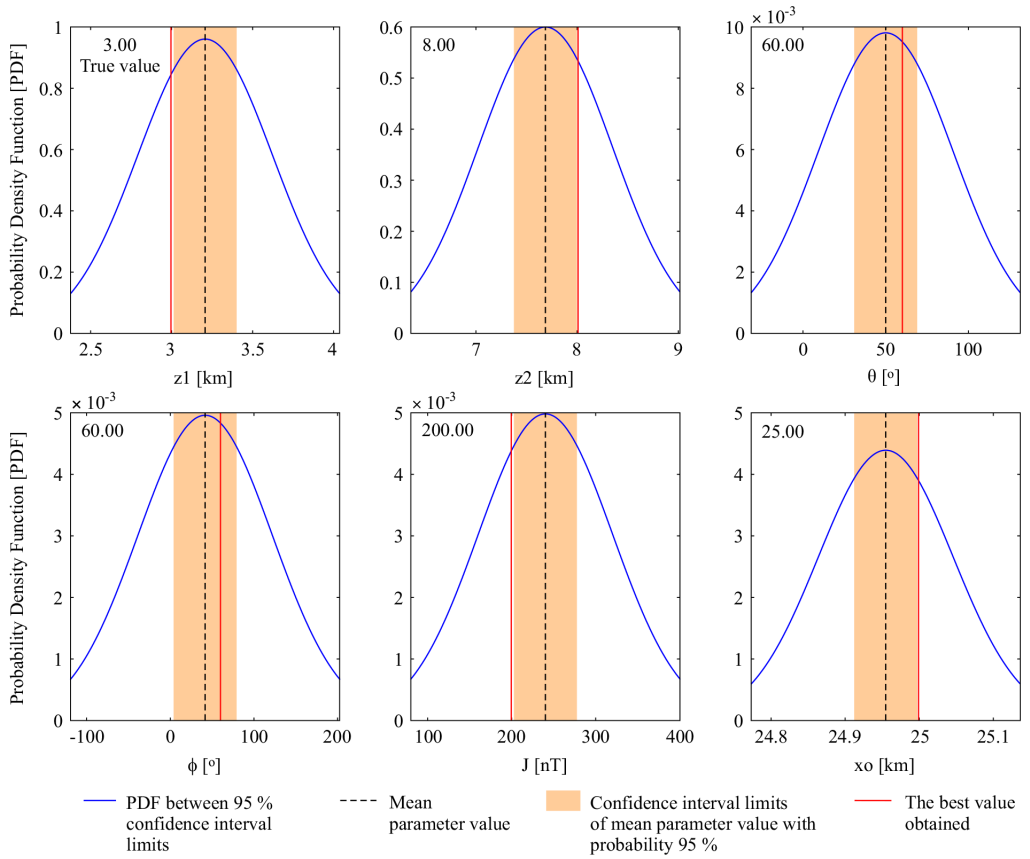

Figure 12. Probability density function analyses of the best model parameter values obtained in 20 independent runs via PSO algorithm for the noise-free magnetic data example. True values of the model parameters are also indicated on each plot.

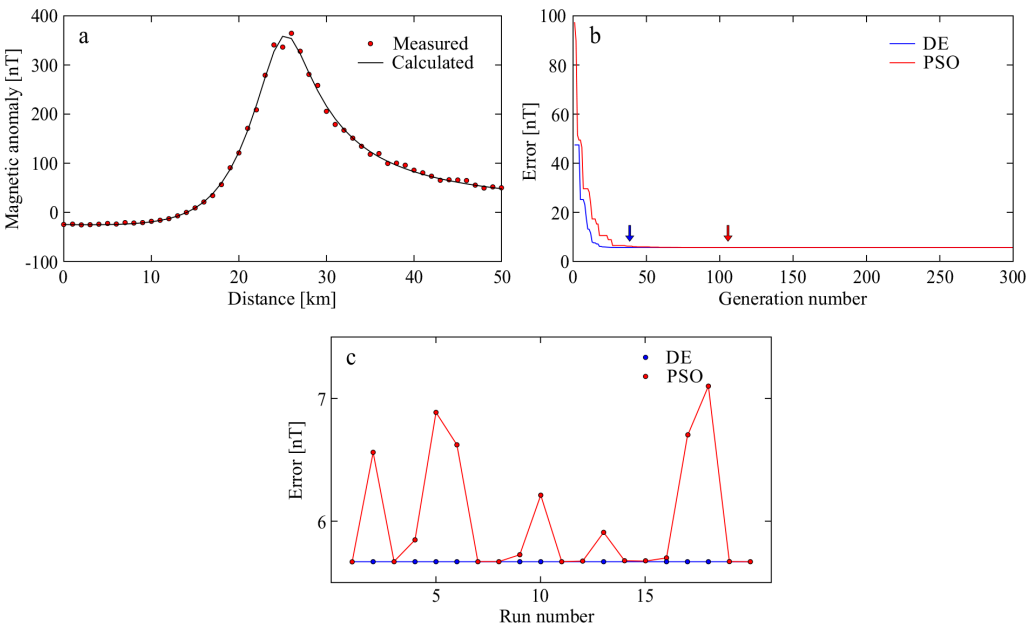

Figure 13. a) The fit between the synthetic noisy magnetic data and the calculated magnetic data obtained from best-fitting model parameters. It must be noted that the DE and PSO algorithms produced almost identical calculated anomalies. b) The change of the error values versus generation number. The arrows show the generation numbers at which the best solutions were obtained. c) The error values obtained from 20 independent runs through DE and PSO algorithms.

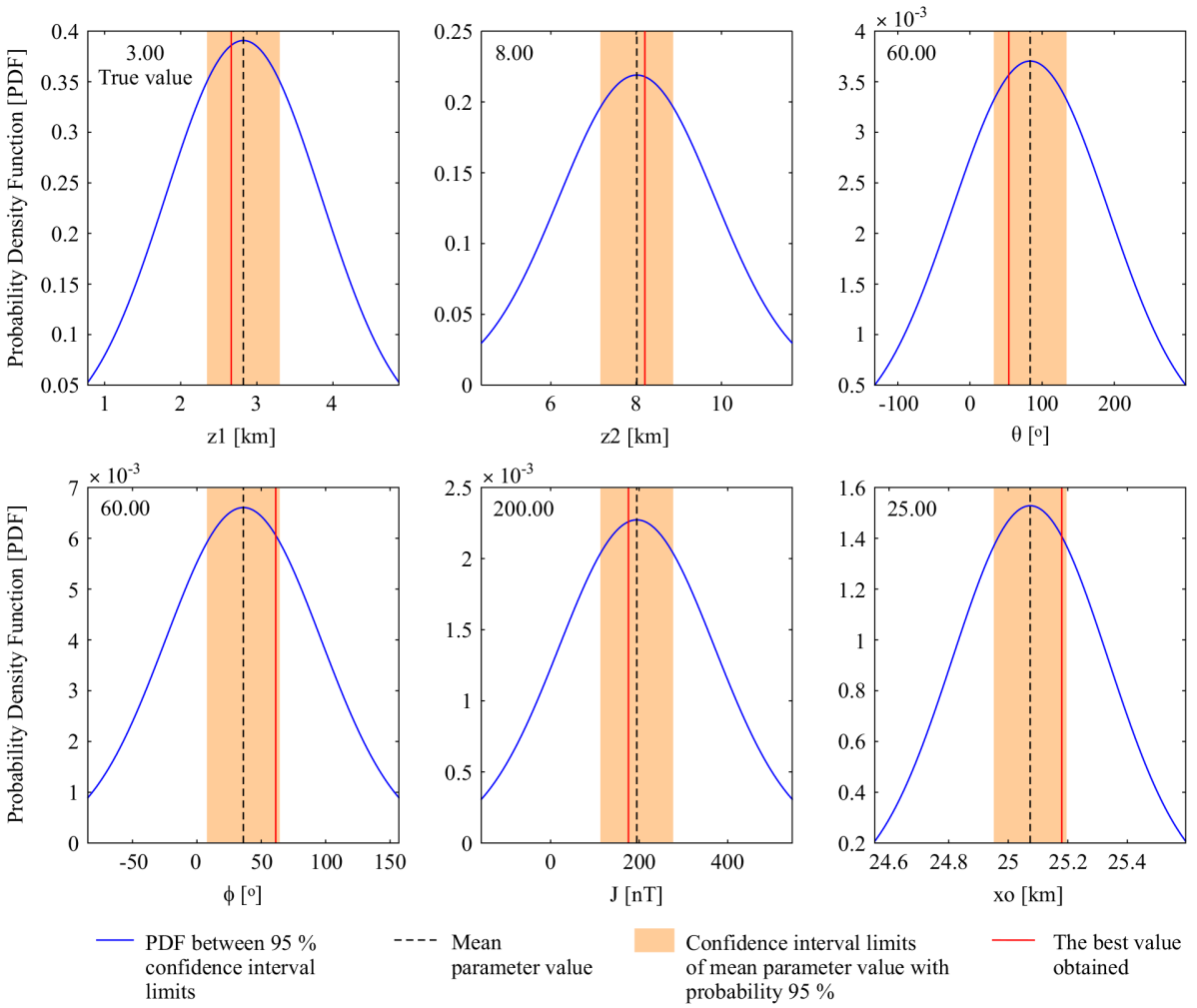

Figure 14. Probability density function analyses of the best model parameter values obtained in 20 independent runs via PSO algorithm for the noisy magnetic data example. True values of the model parameters are also indicated on each plot.

Table 9. Search space bounds and estimated parameter values for the gravity data of Garber oil field, USA. Best and mean represent the optimum and mean solutions obtained from 20 independent runs.

Model parameters	Search spaces		Estimated values					
	Min.	Max.	DE		PSO			
			Best	Mean	Best	Mean	A	B
z1 [km]	0.10	2.00	0.58	0.69 ± 0.25	0.74	1.39 ± 0.68	0.99	0.62
z2 [km]	2.00	10.00	3.77	3.60 ± 0.35	3.52	2.78 ± 0.94	2.80	3.29
θ [°]	0.01	180.00	84.73	81.55 ± 7.05	81.80	105.25 ± 30.02		
dc [g cm^{-3}]	0.01	0.50	0.017	0.02 ± 0.01	0.02	0.038 ± 0.03		
xo [km]	0.01	20.00	7.86	7.89 ± 0.07	7.90	7.82 ± 0.24		
Error [mGal]			0.009		0.010			
CPU time (s)			98.20		423.50			

A represents the results of Radhakrishna Murty and Krishnamacharyulu (1990).
B represents the results of Malleswara Rao et al. (2003).

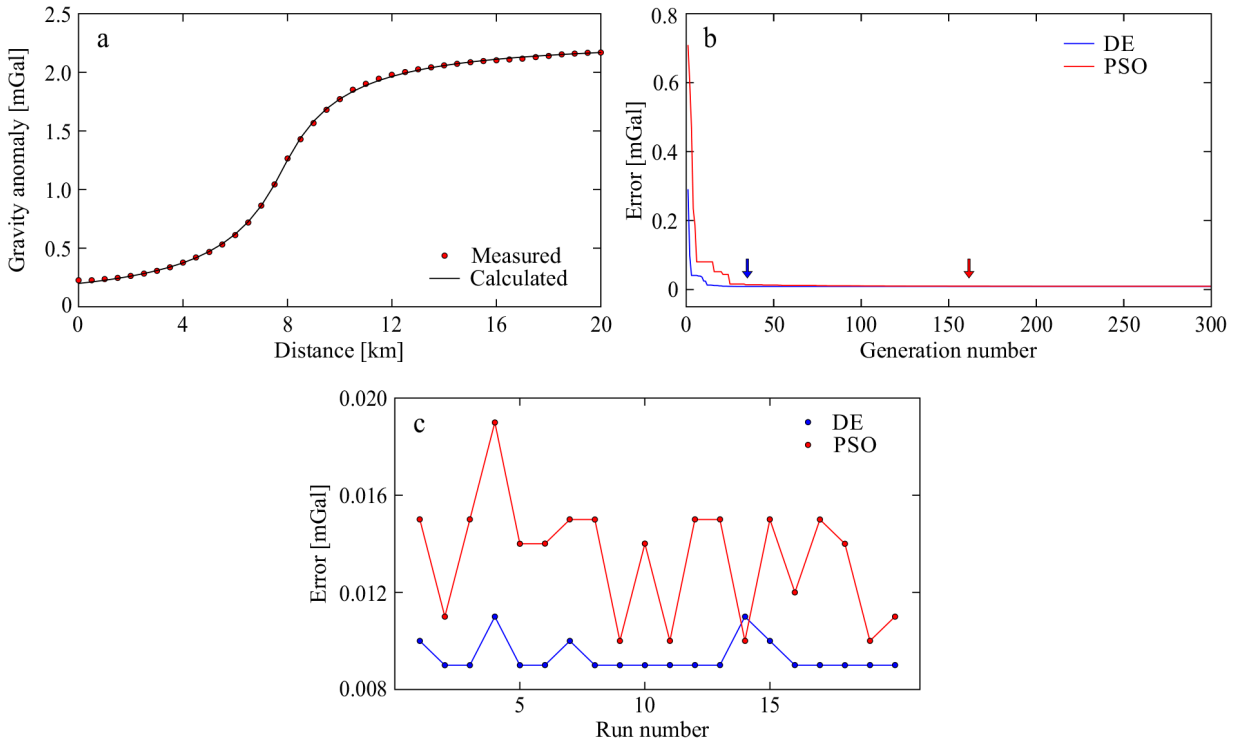

Figure 15. a) The fit between the Garber oil field (USA) residual gravity data and the calculated gravity data obtained from best-fitting model parameters. It must be noted that the DE and PSO algorithms provided almost identical calculated anomalies. b) The change of the error values versus generation number. The arrows show the generation numbers at which the best solutions were obtained. c) The error values obtained from 20 independent runs through DE and PSO algorithms.

Table 10. Search space bounds and estimated parameter values for the magnetic data of Perth Basin, Australia. Best and mean represent the optimum and mean solutions obtained from 20 independent runs.

Model parameters	Search spaces		Estimated values					
	Min.	Max.	DE		PSO		A	B
			Best	Mean	Best	Mean		
z1 [km]	0.10	10.00	5.10	5.10	5.34	5.62 ± 1.70	6.30–6.85	6.21
z2 [km]	10.00	20.00	13.76	13.76	13.32	10.49 ± 8.21	15.55–16.50	15.07
θ [°]	0.01	180.00	141.13	141.13	142.10	108.41 ± 77.39		
ϕ [°]	–180.00	180.00	–14.93	–14.93	–14.04	12.90 ± 62.99		
J [nT]	1.00	1000.00	78.53	78.53	84.54	104.46 ± 31.06		
xo [km]	0.01	50.00	17.16	17.16	17.13	17.93 ± 1.52		
Error [nT]			1.21		1.23			
CPU time (s)			129.80		619.80			

A represents the results of Qureshi and Nalaye (1978).
B represents the results of Radhakrishna Murty et al. (2001).

5. Conclusions

Since PSO is known to be robust and rapid in solving nonlinear problems, it is the most commonly used global optimization algorithm in model parameter estimation studies in geophysics. On the other hand, although the DE algorithm has been introduced as a powerful tool

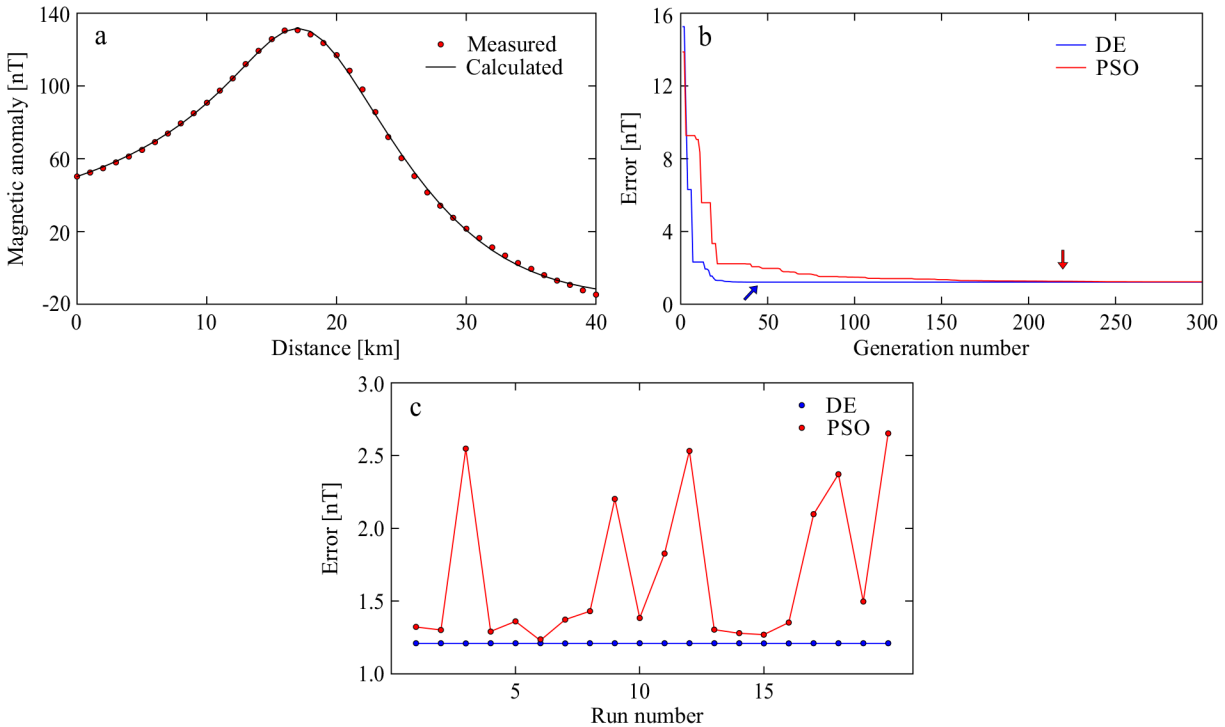

Figure 16. a) The fit between the Perth Basin (Australia) total field magnetic data and the calculated magnetic data obtained from best-fitting model parameters. It must be noted that the DE and PSO algorithms provided almost identical calculated anomalies. b) The change of the error values versus generation number. The arrows show the generation numbers at which the best solutions were obtained. c) The error values obtained from 20 independent runs through DE and PSO algorithms.

for the inversion of potential field datasets in some recent studies, it has not gained enough popularity in geophysical society. Thus, under equal conditions, an attempt was made to compare these two powerful nature-inspired metaheuristic global optimization algorithms in terms of accuracy, computational cost, convergence rate, robustness, and consistency. Optimization studies were performed using both synthetic and real gravity and magnetic anomalies due to deep-seated fault structures. A residual gravity anomaly from the USA and a total field magnetic anomaly from Australia were used for real data experiments.

First, the suitability of the inverse problems under consideration was verified for comparison studies by producing error energy topography maps showing the resolvability characteristics of the model parameters. In order to get optimum efficiency from both algorithms, their best control parameters for gravity and magnetic fault problems were determined through some efficient parameter tuning studies. In the experiments, quite wide search space bounds for the model parameters were used to test their performances. Considering the best solutions of 20 independent runs, PSO and DE algorithms produced very close results in both synthetic and real data examples. However, the mean parameter values of the PSO solutions have relatively high SD values, which indicate that the obtained model parameter values are spread out over a wider range of values. Moreover, PDF plots also indicated some possible uncertainties in the synthetic model parameter estimations performed via PSO. On the other hand, DE showed more robust and consistent performances in every example. Rapid convergence rate and less computational cost are also the main advantages of the DE algorithm. Based on the results of both synthetic and real data experiments presented here, DE is superior to PSO. Hence, the DE algorithm deserves more attention in model parameter studies performed with geophysical potential field methods.

Acknowledgments

The authors thank three anonymous reviewers for their many constructive comments, which greatly improved the earlier version of the paper. A part of this paper was presented at the International Earth Science Colloquium on the Aegean Region (IESCA 2019), October 07–11, 2019, İzmir, Turkey. Scilab 5.5.1, free and open-source software (distributed under CeCILL license-GPL compatible) developed by Scilab Enterprises (http://www.scilab.org), was used for the computations.

References

Alkan H, Balkaya Ç (2018). Parameter estimation by Differential Search Algorithm from horizontal loop electromagnetic (HLEM) data. Journal of Applied Geophysics 149: 77-94.

Asfahani J, Tlas M (2007). A robust nonlinear inversion for the interpretation of magnetic anomalies caused by faults, thin dikes and spheres like structure using stochastic algorithms. Pure and Applied Geophysics 164: 2023-2042.

Aydemir A, Ates A, Bilim F, Buyuksarac A, Bektas O (2014). Evaluation of gravity and aeromagnetic anomalies for the deep structure and possibility of hydrocarbon potential of the region surrounding Lake Van, eastern Anatolia, Turkey. Surveys in Geophysics 35: 431-448.

Balkaya Ç (2013). An implementation of differential evolution algorithm for inversion of geoelectrical data. Journal of Applied Geophysics 98: 160-175.

Balkaya Ç, Ekinci YL, Göktürkler G, Turan S (2017). 3D non-linear inversion of magnetic anomalies caused by prismatic bodies using differential evolution algorithm. Journal of Applied Geophysics 136: 372-386.

Balkaya Ç, Göktürkler G, Erhan Z, Ekinci YL (2012). Exploration for a cave by magnetic and electrical resistivity surveys: Ayvacık Sinkhole Example, Bozdağ İzmir (Western Turkey). Geophysics 77: B135-B146.

Başokur AT, Akça I, Siyam NWA (2007). Hybrid genetic algorithms in view of the evolution theories with application for the electrical sounding method. Geophysical Prospecting 55: 393-406.

Biswas A (2015). Interpretation of residual gravity anomaly caused by a simple shaped body using very fast simulated annealing global optimization. Geoscience Frontiers 6: 875-893.

Biswas A (2017). A review on modeling, inversion and interpretation of self-potential in mineral exploration and tracing paleo-shear zones. Ore Geology Reviews 91: 21-56.

Biswas A, Acharya T (2016). A very fast simulated annealing method for inversion of magnetic anomaly over semi-infinite vertical rod-type structure. Modeling Earth System and Environment 2: 198.

Biswas A, Parija MP, Kumar S (2017). Global nonlinear optimization for the interpretation of source parameters from total gradient of gravity and magnetic anomalies caused by thin dyke. Annals of Geophysics 60: G0218.

Biswas A, Sharma SP (2014). Optimization of self-potential interpretation of 2-D inclined sheet-type structures based on very fast simulated annealing and analysis of ambiguity. Journal of Applied Geophysics 105: 235-247.

Boukerbout H, Abtout A, Gibert D, Henry B, Bouyahiaoui B et al. (2018). Identification of deep magnetized structures in the tectonically active Chlef area (Algeria) from aeromagnetic data using wavelet and ridgelet transforms. Journal of Applied Geophysics 154: 167-181.

Büyüksaraç A, Jordanova D, Ateş A, Karloukovski V (2005). Interpretation of the gravity and magnetic anomalies of the Cappadocia Region, Central Turkey. Pure and Applied Geophysics 162: 2197-2213.

Carlisle A, Dozier G (2001). An off-the-shelf PSO. In: Proceedings of the Workshop on Particle Swarm Optimization, Indianapolis, IN, USA, pp. 1-6.

Chen C, Xia J, Liu J, Feng G (2006). Nonlinear inversion of potential field data using a hybrid-encoding genetic algorithm. Computers and Geosciences 32: 230-239.

Chunduru RK, Sen MK, Stoffa PL (1997). Hybrid optimization for geophysical inversion. Geophysics 62: 1196-1207.

Damaceno JG, de Castro DL, Valcácio SN, Souza ZS (2017). Magnetic and gravity modeling of a Paleogene diabase plug in Northeast Brazil. Journal of Applied Geophysics 136: 219-230.

Das S, Abraham A, Konar A (2008). Particle swarm optimization and differential evolution algorithms: technical analysis, applications and hybridization perspectives. Studies in Computational Intelligence 116: 1-38.

Duan HB, Liu SQ (2010). Non-linear dual-mode receding horizon control for multiple unmanned air vehicles formation flight based on chaotic particle swarm optimisation. Control Theory and Applications 4: 2565-2578.

Eberhart RC, Y Shi (2000). Comparing inertia weights and constriction factors in particle swarm optimization. In: Proceedings of the 2000 Congress on Evolutionary Computation. New York, NY, USA: IEEE.

Eiben AE, Smit SK (2011). Parameter tuning for configuring and analyzing evolutionary algorithms. Swarm and Evolutionary Computation 1: 19-31.

Ekinci YL (2008). 2D focusing inversion of gravity data with the use of parameter variation as a stopping criterion. Journal of the Balkan Geophysical Society 11: 1-9.

Ekinci YL (2016). MATLAB-based algorithm to estimate depths of isolated thin dike-like sources using higher-order horizontal derivatives of magnetic anomalies. SpringerPlus 5: 1384.

Ekinci YL, Balkaya Ç, Göktürkler G, Turan S (2016). Model parameter estimations from residual gravity anomalies due to simple-shaped sources using differential evolution algorithm. Journal of Applied Geophysics 129: 133-147.

Ekinci YL, Demirci A (2008). A damped least-squares inversion program for the interpretation of Schlumberger sounding curves. Journal of Applied Sciences 8: 4070-4078.

Ekinci YL, Ertekin C, Yiğitbaş E (2013). On the effectiveness of directional derivative based filters on gravity anomalies for source edge approximation: synthetic simulations and a case study from the Aegean Graben System (Western Anatolia, Turkey). Journal of Geophysics and Engineering 10 (3): 035005.

Ekinci YL, Özyalın Ş, Sındırgı P, Balkaya G, Göktürkler G (2017). Amplitude inversion of 2D analytic signal of magnetic anomalies through differential evolution algorithm. Journal of Geophysics and Engineering 14: 1492-1508.

Ekinci YL, Yiğitbaş EA (2012). Geophysical approach to the igneous rocks in the Biga Peninsula (NW Turkey) based on airborne magnetic anomalies: geological implications. Geodinamica Acta 25: 267-285.

Ekinci YL, Yiğitbaş E (2015). Interpretation of gravity anomalies to delineate some structural features of Biga and Gelibolu peninsulas, and their surroundings (north-west Turkey). Geodinamica Acta 27: 300-319.

Essa KS (2012). A fast interpretation method for inverse modelling of residual gravity anomalies caused by simple geometry. Journal of Geological Research 2012: 327037.

Essa KS, Elhussein M (2018). PSO (Particle Swarm Optimization) for interpretation of magnetic anomalies caused by simple geometric structures. Pure and Applied Geophysics 175: 3539-3553.

Essa KS, Munschy M (2019). Gravity data interpretation using the particle swarm optimization method with application to mineral exploration. Journal of Earth System Science 128: 123.

Fedi M, Rapolla A (1999). 3-D inversion of gravity and magnetic data with depth resolution. Geophysics 64: 452-460.

Ferris C (1987). Gravity anomaly resolution at the Garber field. Geophysics 52: 1570-1579.

Fernández-Martínez JL, García-Gonzalo E, Fernández Álvarez JP, Kuzma HA, Menéndez Pérez CO (2010). PSO: a powerful algorithm to solve geophysical inverse problems. Application to a 1D-DC resistivity case. Journal of Applied Geophysics 71: 13-25.

Gallardo LA, Meju MA (2004). Joint two-dimensional dc resistivity and seismic travel-time inversion with cross-gradients constraints. Journal of Geophysical Research 109: B03311.

Göktürkler G, Balkaya Ç (2012). Inversion of self-potential anomalies caused by simple geometry bodies using global optimization algorithms. Journal of Geophysics and Engineering 9: 498-507.

Grant FS, West GF (1965). Interpretation Theory in Applied Geophysics: New York, NY, USA: McGraw Hill Book Co.

Jiang M, Luo YP, Yang SY (2007). Stochastic convergence analysis and parameter selection of the standard particle swarm optimization algorithm. Information Processing Letters 102 (1): 8-16.

Kaftan İ (2017). Interpretation of magnetic anomalies using a genetic algorithm. Acta Geophysica 65: 627-634.

Kennedy J, Eberhart R (1995). Particle swarm optimization. In: IEEE International Conference on Neural Networks. New York, NY, USA: IEEE, pp. 1942-1948.

Li Y, Oldenburg DW (1996). 3-D inversion of magnetic data. Geophysics 61: 394-408.

Malleswara Rao MM, Ramana Murty TV, Murthy KSR, Vasudeva RY (2003). Application of natural generalised inverse technique in reconstruction of gravity anomalies due to a fault. Indian Journal of Pure and applied Mathematics 34: 31-47.

Maiti S, Gupta G, Erram VC, Tiwari RK (2011). Inversion of Schlumberger resistivity sounding data from the critically dynamic Koyna region using the hybrid Monte Carlo-based neural network approach. Nonlinear Process in Geophysics 18: 179-192.

Mehanee SA (2014). Accurate and efficient regularized inversion approach for the interpretation of isolated gravity anomalies. Pure and Applied Geophysics 171: 1897-1937.

Mehanee S, Essa KS (2015). 2.5D regularized inversion for the interpretation of residual gravity data by a dipping thin sheet: numerical examples and case studies with an insight on sensitivity and non-uniqueness. Earth, Planets and Space 67: 130.

Mehanee S, Essa KS, Smith PD (2011). A rapid technique for estimating the depth and width of a two-dimensional plate from self-potential data. Journal of Geophysics and Engineering 8: 447-456.

Menke W (1989). Geophysical Data Analysis – Discrete Inverse Theory. San Diego, CA, USA: Academic Press.

Montesinos FG, Arnoso J, Viera R (2005). Using a genetic algorithm for 3-D inversion of gravity data in Fuerteventura (Canary Islands). International Journal of Earth Sciences 94: 301-316.

Monteiro Santos FA (2010). Inversion of self-potential of idealized bodies' anomalies using particle swarm optimization. Computer and Geosciences 36: 1185-1190.

Montesinos FG, Blanco-Montenegro I, Arnoso J (2016). Three-dimensional inverse modelling of magnetic anomaly sources based on a genetic algorithm. Physics of the Earth and Planetary Interiors 253: 74-87.

Nagihara S, Hall SA (2001). Three-dimensional gravity inversion using simulated annealing: constraints on the diapiric roots of allochthonous salt structures. Geophysics 66: 1438-1449.

Ogunbo JN (2018). MATLAB code for data-driven initial model of 1D Schlumberger sounding curve. Geophysics 83: F21-F28.

Oruç B, Gomez-Ortiz D, Petit C (2017). Lithospheric flexural strength and effective elastic thickness of the Eastern Anatolian (Turkey) and surrounding region. Journal of Asian Earth Sciences 150: 1-13.

Oruç B, Keskinsezer A (2008). Detection of causative bodies by normalized full gradient of aeromagnetic anomalies from east Marmara region, NW Turkey. Journal of Applied Geophysics 65: 39-49.

Pallero JLG, Fernandez-Martinez JL, Bonvalot S, Fudym O (2015). Gravity inversion and uncertainty assessment of basement relief via particle swarm optimization. Journal of Applied Geophysics 116: 180-191.

Pallero JLG, Fernandez-Martinez JL, Bonvalot S, Fudym O (2017). 3D gravity inversion and uncertainty assessment of basement relief via particle swarm optimization. Journal of Applied Geophysics 139: 338-350.

Pekşen E, Yas T, Kayman AY, Özkan C (2011). Application of particle swarm optimization on self-potential data. Journal of Applied Geophysics 75: 305-318.

Pekşen E, Yas T, Kıyak A (2014). 1-D DC resistivity modeling and interpretation in anisotropic media using particle swarm optimization. Pure and Applied Geophysics 171: 2371-2389.

Qureshi IP, Nalaye AM (1978). A method for direct interpretation of magnetic anomalies caused by 2-d vertical faults. Geophysics 43: 179-188.

Radhakrishna Murthy IV (1998). Gravity and Magnetic Interpretation in Exploration Geophysics. Bangalore, India: Geological Society of India.

Radhakrishna Murthy IV, Krishnamacharyulu SKG (1990). Automatic inversion of gravity anomalies of faults. Computer and Geosciences 16: 539-548.

Radhakrishna Murthy IV, Swamy KV, Jagannadha Rao S (2001). Automatic inversion of magnetic anomalies of faults. Computer and Geosciences 27: 315-325.

Roy L, Sen MK, Blankenship D, Stoffa PL, Richter T (2005). Inversion and uncertainty estimation of gravity data using simulated annealing: an application over Lake Vostok, East Antarctica. Geophysics 70: J1-J12.

Salem A, Ravat D, Mushayandebvu MF, Ushijima K (2004). Linearized least-squares method for interpretation of potential field data from sources of simple geometry. Geophysics 69: 783-788.

Sen M, Stoffa PL (1995). Global Optimization Methods in Geophysical Inversion. Volume 4 of Advances in Exploration Geophysics. Amsterdam, the Netherlands: Elsevier.

Sharma SP, Biswas A (2013). Interpretation of self-potential anomaly over a 2D inclined structure using very fast simulated-annealing global optimization - an insight about ambiguity. Geophysics 78: WB3–WB15.

Shi Y, Eberhart RC (1998). Parameter selection in particle swarm optimization. In: Proceedings of the 7th International Conference on Evolutionary Programming, VII, New York, NY, USA, pp. 591-600.

Sındırgı P, Özyalın Ş (2019). Estimating the location of a causative body from a self-potential anomaly using 2D and 3D normalized full gradient and Euler deconvolution. Turkish Journal of Earth Sciences 28: 640-659.

Singh A, Biswas A (2016). Application of global particle swarm optimization for inversion of residual gravity anomalies over geological bodies with idealized geometries. Natural Resources Research 25: 297-314.

Srivastava S, Agarwal BNP (2010). Inversion of the amplitude of the two-dimensional analytic signal of magnetic anomaly by the particle swarm optimization technique. Geophysical Journal International 182: 652-662.

Storn R (1996). On the usage of differential evolution for function optimization. In: 1996 Biennial Conference North American Fuzzy Information Processing Society, Berkeley, CA, USA, pp. 519-523.

Storn R, Price K (1995). Differential Evolution – A Simple and Efficient Adaptive Scheme for Global Optimization over Continuous Spaces. Technical Report TR-95-012. Berkeley, CA, USA: International Computer Science Institute.

Storn R, Price K (1997). Differential evolution — a simple and efficient heuristic for global optimization over continuous spaces. Journal of Global Optimization 11: 341-359.

Tarantola A (2005). Inverse Problem Theory and Methods for Model Parameter Estimation. Philadelphia, PA, USA: Society of Industrial and Applied Mathematics.

Timur E, Kaftan İ, Sarı C, Şalk M (2019). Structure of the Büyük Menderes Graben systems from gravity anomalies. Turkish Journal of Earth Sciences 28: 544-557.

Tlas M, Asfahani J (2011). Fair function minimization for interpretation of magnetic anomalies due to thin dikes, spheres and faults. Journal of Applied Geophysics 75: 237-243.

Toushmalani R (2013). Comparison result of inversion of gravity data of a fault by particle swarm optimization and Levenberg-Marquardt methods. SpringerPlus 2: 462.

Trelea IC (2003). The particle swarm optimization algorithm: convergence analysis and parameter selection. Information Processing Letters 85: 317-325.

Xu Y, Hao T, Zhao B, Lihong Z, Zhang L et al. (2011). Investigation of igneous rocks in Huanghua depression, North China, from magnetic derivative methods. Journal of Geophysics and Engineering 8: 74-82.

Yamamoto M, Seama N (2004). Genetic algorithm inversion of geomagnetic vector data using a 2.5-dimensional magnetic structure model. Earth, Planets and Space 56: 217-227.